Thinning mechanisms of heterogeneous continental lithosphere

Benoit Petri, Thibault Duretz, Geoffroy Mohn, Stefan M Schmalholz, Garry D. Karner, Othmar Müntener

Thinning mechanisms of heterogeneous continental lithosphere

Benoît PETRI[1*], Thibault DURETZ[1,2], Geoffroy MOHN[3], Stefan M. SCHMALHOLZ[1], Garry D. KARNER[4], Othmar MÜNTENER[1]

[1] *Institute of Earth Sciences, University of Lausanne, Géopolis, 1015 Lausanne, Switzerland*
[2] *Univ Rennes, CNRS, Géosciences Rennes UMR 6118, F-35000 Rennes, France*
[3] *Département Géosciences et Environnement, Université de Cergy-Pontoise, 5, mail Gay Lussac, Neuville-sur-Oise, 95031 Cergy-Pontoise Cedex, France*
[4] *ExxonMobil Exploration Company, 22777 Springwoods Village Pkwy, Spring, Houston, TX-77389, USA*

*Corresponding author: bpetri@unistra.fr

ORCID Petri: 0000-0001-7142-0406
ORCID Duretz: 0000-0001-8472-7490
ORCID Mohn: 0000-0002-8729-2960
ORCID Schmalholz: 0000-0003-4724-2181
ORCID Müntener: 0000-0002-7771-4381
ORCID Karner: /

HIGHLIGHTS

- Pre-rift architecture of the continental lithosphere is important during rifting
- Initial mechanical heterogeneities control strain partitioning
- Extraction tectonics is an efficient thinning mechanism
- Various crustal levels can be exhumed in distal margins

KEYWORDS

- Rifting
- Rifted margin
- Lithospheric thinning
- Extraction tectonics
- Inheritance

ABSTRACT

The mechanisms responsible for the formation of extremely thinned continental crust (< 10 km thick) and lithosphere during rifting remains debated. Observations from present-day and fossil passive margins highlight the role of deep-seated deformation, likely controlled by heterogeneities within the continental lithosphere, such as changing lithologies, mechanical anisotropies and inherited structures. We investigate the mechanisms of lithospheric thinning by exploring the role of pre-existing heterogeneities on the architecture and evolution of rifted margins. We estimate pre-rift pressure conditions (P_0) vs. depth diagrams of crustal to lithospheric sections, to quantify rift-related modifications on inherited lithostatic pressure gradients. Two field examples from the Alpine Tethys margins in the Eastern and Southern Alps (SE Switzerland and N Italy) were selected to characterize: (1) the pre-rift architecture of the continental lithosphere; (2) the localization of rift-related deformation in distinct portions of the lithosphere; and (3) the interaction between pre-

existing heterogeneities of the lithosphere and rift-related structures. These observations are compared with high-resolution, two-dimensional thermo-mechanical numerical models. The design of the models takes into account pre-existing mechanical heterogeneities representing the initial pre-rift architecture of the continental lithosphere. Extensional structures consist of high-angle and low-angle normal faults, anastomosing shear-zones and decoupling horizons. Such structures accommodate the lateral extraction of mechanically stronger levels derived from the middle to lower crust. As a result, the extremely thinned continental crust in Tethyan passive margins represents the juxtaposition and amalgamation of distinct strong levels of the crust separated by major extensional structures identified by sharp pressure gradients. Future work should determine the applicability of these results to other present-day and fossil rifted margins.

GRAPHICAL ABSTRACT

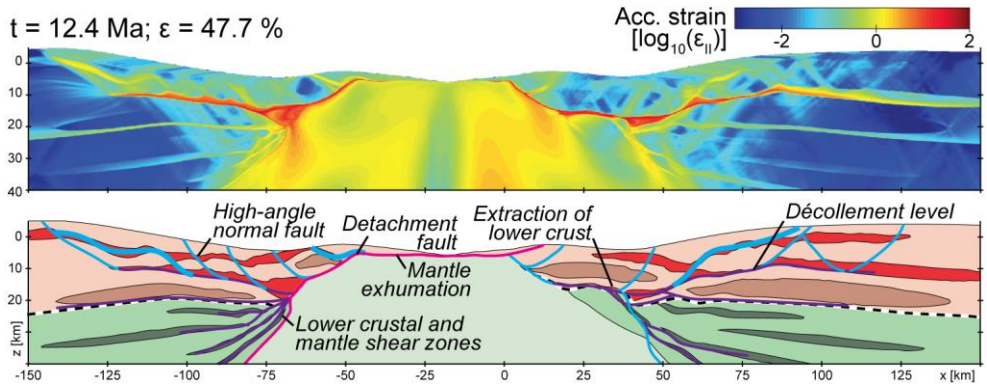

1. INTRODUCTION

The increased number of high-quality geophysical surveys across continental rifted margins has allowed to recognize the characteristic first-order architecture of margins. Commonly, rifted margins that approach break-up are the result of extreme crustal and lithospheric thinning. The crustal thickness typically passes from 30-35 km to less than 10 km over a distance of a hundred kilometers (e.g. Osmundsen and Ebbing, 2008). Reflection seismic data indicate that the deformation of upper crustal levels is achieved through high-angle and low-angle normal faulting (e.g. Whitmarsh et al., 2000), but attempts to restore displacements accommodated along these brittle, upper-crustal extensional structures fail in explaining the observed amount of lithospheric thinning (e.g., Kusznir and Karner, 2007; Reston, 2007a). Deep, intra-basement deformation likely plays a critical role in such extreme crustal and lithospheric thinning (Huismans and Beaumont, 2014; Karner et al., 2003). The direct characterization of this deeper deformation remains elusive in present-day rifted margins and has only been described for a small number of margins (Clerc et al., 2018, 2015; Reston, 1988). In contrast, many conceptual models have been proposed for a wide range of deformation styles involving, among others, oceanward or continentward lower crustal "flow" and crustal necking (Reston, 2007b).

Indeed, contrary to the upper crustal deformation, the localization, partitioning, and deformation style of extensional structures at depth may be controlled by the lithological, structural and thermal state of the continental lithosphere (e.g. Duretz et al., 2016b). The spatial and temporal heterogeneity of the lithosphere, having various petrological, chemical, mechanical and thermal characteristics, has been noted in some places (Rader et al., 2015; Thybo and Artemieva, 2013) as well as its impact on the architecture and evolution of rifted margins (e.g. Tommasi and Vauchez, 2001; Zastrozhnov et al., 2018). However, their detailed

role and influence on the mechanisms of crustal and lithospheric stretching and thinning remain elusive.

The objective of this contribution is to investigate the mechanisms of extreme lithospheric thinning by exploring the role of initial or pre-existing mechanical heterogeneities on the architecture and evolution of passive margins by comparing field-derived observations and quantification to numerical models. In contrast to present-day rifted margins, deep extensional, exposed rift-related structures have been mapped and can be accessed in fossil equivalents preserved in present-day orogens. Field observations from the Alps in Western Europe preserving the Alpine Tethys remnants enable us to characterize and describe the first-order relations between rift-related structures and the initial heterogeneities of the continental lithosphere. These observations are subsequently incorporated into high-resolution, two-dimensional thermo-mechanical numerical models of lithospheric extensional deformation.

2. APPROACH

The characterization of rift-related, intra-basement deformation relies on being able to sample rocks of the extended continental lithosphere. In particular, exposure of distinct portions of the continental lithosphere is possible when rifted margins have been thrusted and uplifted in orogens (Beltrando et al., 2014; Dewey and Bird, 1970). There, under certain conditions, the pre-, syn- and post-rift history can be determined (Beltrando et al., 2013; Frasca et al., 2016; Mohn et al., 2010) from both the stratigraphic and basement evolution (Fig. 1). However, investigating the role of initial heterogeneities during rifting requires key prerequisites: (1) recognition of rift-related structures from pre- and post-rift (i.e. orogenic, post-orogenic) structures; and (2) detailed pressure – temperature – time – deformation (*P-T-t-d*) evolution of distinct portions of the continental lithosphere.

The Alps, preserving the remnants of the Alpine Tethys margins, satisfy these requirements. More than a century of research in these areas permits the recognition of rift

structures related to the opening of the Alpine Tethys and its evolution (see Mohn et al., 2010 for a review). Here, we focus on the remnants of the Alpine Tethys preserved in the Eastern Alps (SE Switzerland and N Italy, Fig. 2ab) and in the Southern Alps (N Italy, Fig. 2ac). These portions of the fossil Adriatic margin have been reactivated and incorporated into the Alpine orogen during the Cretaceous to Oligocene/Miocene but escaping significant Alpine deformation and metamorphic overprint (Fig. 2bc; see Mohn et al., 2011 for the Central Alps; Schmid et al., 1987; Wolff et al., 2012 for the Southern Alps).

The Paleozoic basement sampled in both the Eastern and Southern Alps records a protracted, polyphase tectonic history. After crustal amalgamation and accretion during the Devonian and Carboniferous Variscan phases (von Raumer et al., 2013), the continental lithosphere underwent a major reorganization during the late Carboniferous and early Permian (e.g. Petri et al., 2017) during which the continental crust returned back to an equilibrated thickness (30-35 km). Extensional tectonics, together with mantle-derived magmatic under- and intra-plating, caused differentiation of the continental crust with granulite, amphibolite and greenschist facies rocks in the lower, middle and upper crust, respectively (Schuster and Stüwe, 2008). Although diffuse and low-magnitude Triassic rifting is locally documented (e.g. Bertotti et al., 1993), no evidence for major exhumation and thinning of the continental lithosphere from the Permian post-orogenic event until the Jurassic rifting has been described. This conclusion is based on two key arguments: (1) isobaric cooling was reported for Permian magmatism and associated contact metamorphism (Müntener et al., 2000; Petri et al., 2016); and (2) the Triassic stratigraphic record, consisting of fluvial to shallow-marine deposits, precludes any major crustal thinning during this time. Therefore, we consider the late Carboniferous and early Permian magmatic intrusions and associated metamorphism as points of reference in terms of their exhumation history during Jurassic rifting.

131 The depth of these magmatic intrusions, and the associated contact metamorphism,
132 have been determined by many studies across the Alps (see Spalla et al., 2014 for a review).
133 Such datasets provide approximate pre-rift pressure conditions (P_0) for the magmatic and
134 metamorphic rocks prior to Jurassic exhumation. Using an average continental crust density
135 (2.7-3.0 $g.cm^{-3}$; Fountain and Salisbury, 1981), the pre-rift architecture of the Alpine
136 basement can be locally reconstructed (A-A' on Fig. 1b) and rift-related pressure effects in the
137 crust can be tracked: in a pre-rift section, data are aligned along an average lithostatic gradient
138 (0.26-0.29 $kbar.km^{-1}$) while rift-related extension modifies the inherited P_0-depth gradients
139 generating either jumps in P_0 with depth (sharp gradient, e.g., missing middle crust) or an
140 increased gradient if deformation is "homogeneously" distributed during thinning (e.g.
141 "ductile flow"; B-B' on Fig. 1b). Such information on pressure gradients can be extracted
142 from both field observations and numerical models. These approaches will be applied to two
143 sections across the reconstructed Jurassic Adriatic rift margin from the proximal to the distal
144 domains. The field observations and associated P_0-depth gradients (see Tables S1 and S2 for
145 full P_0 dataset) will be compared with results of numerical simulations in order to propose a
146 model for the evolution and mechanisms of continental lithosphere thinning of the Alpine
147 Tethys rifted margins.

148 **3. THE EASTERN ALPS CASE STUDY**

149 The Eastern Alps preserved the remnants of the Adriatic rifted margin that has been
150 variably reactivated during the Alpine orogeny from Late Cretaceous to Tertiary (Figs. 2ab-4;
151 Froitzheim et al., 1994; Mohn et al., 2011). Two distinct Alpine nappe stacks have been
152 identified and are separated by the Lunghin-Mortirolo Movement Zone (LMMZ). To the
153 north, the Err - Platta and Campo - Grosina nappe stacks underwent minor to moderate Alpine
154 overprint with metamorphic conditions that did not exceed greenschist facies conditions
155 (Froitzheim et al., 1994; Mohn et al., 2011). To the south the Bernina - Margna - Sella -

Malenco nappe stack was pervasively deformed and metamorphosed reaching amphibolite facies conditions during the Alpine orogeny (Figs. 2ab, 3a; see Mohn et al., 2011).

Previous studies (Mohn et al., 2012, 2011) recognized, from northeast to west, the proximal domain, the necking zone and the distal domain of the former Adriatic margin (Figs. 2ab, 3) in these two distinct Alpine nappe stacks. Despite variable Alpine metamorphic overprints, rift-related basement deformation has been documented in both the necking zone and distal domain (Fig. 3bc) and are described below.

3.1. Necking Zone: the Campo - Grosina section

The former necking zone (section A-A' on Fig. 3) is composed of pre-rift upper to middle crust, which is represented by the Campo and Grosina units separated by the Eita Shear Zone (ESZ, Fig. 4ab; Mohn et al., 2012). The underlying Campo unit is composed of amphibolite facies metasediments with a main NW-SE striking vertical foliation. These metasediments are intruded by a Permian gabbroic pluton emplaced at 4-6 kbar (Sondalo mafic complex, point 3; Petri et al., 2016). Importantly, the center of the Campo unit is devoid of any significant post-Permian deformation (see Petri et al., 2018). The overlying Grosina unit is made of amphibolite-facies orthogneiss and metasediments of unknown age showing a gently NW-dipping foliation cross cut by numerous greenschist facies extensional shear zones (Fig. 4cd). The ESZ represents a major shear zone that can be mapped over 20 km and is at the same structural interface, i.e., between the Campo and Grosina units (Fig. 3a). Together, these data suggest that the ESZ represents a horizontal mid-crustal extensional shear zone with an age constrained by $^{40}Ar/^{39}Ar$ dating of porphyroclastic micas from the underlying Campo unit at 205-180 Ma (Mohn et al., 2012). The rift-related P_0-depth diagram in this section is characterized by an increased pressure gradient in the Grosina unit with respect to the lithostatic gradient of 0.29 kbar.km^{-1}.

The top of the Grosina unit presents a large-scale brittle detachment fault with cataclasite and pseudotachylite zones corresponding to the Grosina detachment.

3.2. Distal margin: Bernina – Margna – Malenco – Sella section

The southern distal domain (section B-B' on Fig. 3) is composed of juxtaposed pre-rift upper and lower crust as well as subcontinental mantle, represented by the Upper Margna - Sella - Bernina units and the Lower Margna - Malenco units, respectively. These two distinct crustal portions are separated by the Magna shear zone (Bissig and Hermann, 1999). The Malenco unit is made of subcontinental mantle (section B-B', point 5), in contact with a pre-rift lower crust composed of felsic granulite and sealed by the Permian Braccia gabbro (Fig. 4e).). The gabbro and the felsic granulite record 10-12 kbar during emplacement at 281-271 Ma and 8 ± 1 kbar during cooling, respectively (section B-B', points 3 and 4; Hansmann et al., 2001; Müntener et al., 2000). In contrast, the pre-rift upper crust is represented by the Fora gneisses (Upper Margna unit), similar to intrusive rocks from the Bernina unit that record less than 3 kbar at 295-292 Ma (section B-B', point 2; Bissig and Hermann, 1999; Von Quadt et al., 1994) and are covered by Permian to Triassic sediments (section B-B', point 1). Despite a strong Alpine overprint, numerous localized pre-Alpine rift-related shear zones have been described in the Margna unit (Müntener and Hermann, 2001). The most prominent is the Margna shear zone, at the contact between the Lower Margna, including the Permian Fedoz gabbro, and Upper Margna units (Fig. 4f), with a top to the E-SE sense of shear when back-rotated to a pre-Alpine position (Bissig and Hermann, 1999). This structure juxtaposes pre-rift rocks recording pressures of ~3 kbar against 8-12 kbar suggesting that ~25 km of continental crust is lacking across this structure (Hermann and Müntener, 1996). As a result, the P_0-depth diagram of section B-B' displays a sharp gradient across the Margna shear zone highlighting the absence of the middle crust and an increased gradient in the lower Margna unit.

In the Bernina pre-rift upper crustal unit, cataclastic structures have been recognized, sometimes at the top basement and sometimes at the contact between the basement and the pre-rift Triassic cover (section B-B', point 1) and are identified as the Jurassic Bernina low-angle detachment fault (Mohn et al., 2011).

3.3. Distal margin: Err - Platta section

The northern distal margin section (section C-C' on Fig. 3) is composed of pre-rift upper crust and subcontinental mantle from the Err and Platta units, respectively, characterized by a set of Jurassic brittle, low-angle detachment faults referred to as the Err and Jenatsch detachments (Froitzheim and Eberli, 1990; Manatschal and Nievergelt, 1997). Two exhumed mantle types have been recognized in the Platta unit nowadays separated by an Alpine thrust: the upper Platta, made of a sub-continental mantle (Spl-peridotite, section C-C', point 4) and the lower Platta unit, made of refertilized sub-continental mantle (Spl-Pl peridotite, section C-C', point 5; Müntener et al., 2010). This indicates that the two mantle types followed very different thermal evolutions during rifting. The Err unit consists of Permian granitoids emplaced within a polymetamorphic basement below 3 kbar at 292 ± 6 Ma (section C-C', point 3; Büchi, 1994; Von Quadt et al., 1994). The granitoids are covered by Permian volcano-sedimentary deposits dated at 288 ± 2 Ma (section C-C', point 2; Von Quadt et al., 1994). In contrast to the Bernina - Margna - Malenco - Sella nappe stack, no evidence for pre-rift lower crust has been recognized in this section. The top of the Err unit is generally capped by a low-angle Jurassic detachment fault locally following the base of Permian basins filled by volcanoclastic deposits (Fig. 4gh; Epin et al., 2017; Masini et al., 2011). The contact between Lower Err and Upper Platta is interpreted as an Alpine thrust, potentially reactivating a former Jurassic rift related structure (Epin et al., 2017). In a P_0-depth diagram, the transition between points 3 and 4 involves a possible sharp gradient resulting from the absence of middle and lower continental crust.

4. THE SOUTHERN ALPS CASE STUDY

The Southern Alps are delimited by the Tertiary Insubric Line to the northwest and by the Pô plain to the south (Figs. 2ac, 5, 6). They are composed at their western end by two major units: the pre-rift middle to lower crustal Ivrea-Verbano Zone (IVZ), recording the emplacement of a Permian mafic complex within a polymetamorphic basement, and the pre-rift upper crustal Serie Dei Laghi (SDL), capped to the southeast by Permian to Mesozoic sediments of the Lombardian basin. Whereas the IVZ is exhumed and tilted to ~ 90° by the time of Jurassic rifting and the Alpine compression (Siegesmund et al., 2008), the SDL and its associated sedimentary cover show only minor Alpine deformation and metamorphic overprint (i.e. lower greenschist facies condition).

The Southern Alps record evidence for long-lasted extension that started in the Late Triassic and shifted progressively westward during the Middle Jurassic (Bertotti et al., 1993). To the east, fault-bounded rift basins such as the Lombardian basin are filled by shallow-water Triassic to Jurassic deposits representing the Adriatic proximal margin (Fig. 5b; Bertotti et al., 1993). The SDL – IVZ are interpreted as the Adriatic necking zone recording major thinning during Jurassic rifting (Decarlis et al., 2017). The distal domain is preserved in the Canavese zone with evidence for subcontinental mantle exhumation at the seafloor (Beltrando et al., 2015a; Ferrando et al., 2004).

Several deep-crustal extensional structures have been documented in the SDL and the IVZ. The oldest, the Cossato-Mergozzo-Brissago line (CMB) was active during the Permian without evidence for subsequent reactivation and delimits, in places, the SDL from the IVZ (Mulch et al., 2002b). Conversely, two sets of structures interpreted as related to Mesozoic rifting have been documented in the IVZ: (1) deep, high-temperature shear zones such as the Anzola-Rosarolo Shear Zone (ARSZ; e.g. Langone et al., 2018) and (2) the shallower Pogallo Line (PL), marking in places also the contact between the SDL and the IVZ. These structures

are described below using three sections that illustrate the partitioning of rift-related deformation in the pre-rift lower crust (Fig. 5bc). The IVZ being presently tilted to ~ 90°, the P_0-depth diagrams can be approximated by P_0 versus the distance to the Tertiary Insubric line (i.e. moving towards this structure, rocks were deeper in pre-rift crustal section).

4.1. Val Sesia section

The Val Sesia and Val Sessera sections (D-D' on Fig. 5) are composed of Permian gabbros and diorites of the Ivrea Mafic Complex with metasedimentary and peridotite lenses capped by upper amphibolite-facies metasediments (Quick et al., 2003). A dense dataset of Permian *P-T* estimates derived from both igneous and metamorphic rocks define a P_0-distance gradient of 0.36 kbar.km^{-1} (Demarchi et al., 1998). Igneous and metamorphic textures are usually preserved whereas only rare and minor shear zones, potentially related to Jurassic rifting, have been described in this section (Altenberger, 1997).

4.2. Val Strona section

The Val Strona section (E-E' on Fig. 5) is composed of gabbroic dykes and amphibolite to granulite facies metasedimentary rocks. This section preserved pre-Triassic structures, crosscut by several shear zones at distinct crustal levels that are rarely dated. The closest to the Insubric line (i.e., the deepest in a reconstructed section), the meters-thick ARSZ (Fig. 6ab) presents syn-deformational amphibolite to granulite facies conditions (> 650 °C) and is dated at 210-200 Ma (Beltrando et al., 2015b; Brodie et al., 1989). Up-section, above the Permian CMB, the PL is the second major rift-related structure outcropping in the Val Strona section (Fig. 6c). It appears as a tilted ductile shear zone dated at 182 ± 2 Ma (Mulch et al., 2002a) with greenschist facies deformation (Handy, 1987). As a result Permian *P-T* conditions overprinted by these successive rift-related deformations define a P_0-depth gradient of 0.42 kbar.km^{-1} (Henk et al., 1997).

4.3. Valle Cannobina section

In the Valle Cannobina (F-F' on Fig. 5), two major high grade deformation zones (Finero Shear Zones; FSZ) separate the Upper amphibolite-facies metasediments (i.e. the Kinzigite formation), the so-called external gabbro from the "layered internal zone" and associated mantle peridotite (Kenkmann and Dresen, 2002) leaving the contact between the "layered internal zone" and the mantle peridotites (i.e., the petrological Moho) undeformed. The shear zones were active at high temperature (>650 °C), record a normal sense of shear and are dated at 235-200 Ma (Langone et al., 2017, 2018). Further away from the Insubric line, the PL presents amphibolite-facies deformations (Handy, 1987). Altogether, the shear zones juxtapose mantle peridotites, upper and lower crustal rocks on a few kilometers distance, resulting in an extremely high P_0-depth gradient of 1.8 kbar.km^{-1} (Handy et al., 1999). This indicates that major crustal thinning occurred at 235-200 Ma along this transect (Handy et al., 1999; Langone et al., 2018) whereas no deformation was documented in the upper-crustal SDL.

5. NUMERICAL MODELING

5.1. Modeling approach

In order to unravel the impact of mechanical heterogeneities on the structuring and architecture of rifted margins, we have designed a set of thermo-mechanical numerical models. The two-dimensional models were carried out at the scale of the continental lithosphere and incorporated discrete km-scale elliptical bodies of differing rheologies that represent inherited lithological variations. The modeling approach is based on a finite difference/marker-in-cell discretization of the momentum and heat transfer equations (Gerya and Yuen, 2003). The numerical algorithm has the ability to simulate the evolution of a true free surface (Duretz et al., 2016a) and combines, in a consistent manner, a variety of

rheological behaviors (elasticity, viscosity, plasticity) and creep mechanisms (Popov and Sobolev, 2008; Schmalholz and Duretz, 2017). See Text S3 for details.

5.2. Model configuration

The initial model domain is 300 km wide and 120 km high (Fig. 7a). Extension is applied by prescribing horizontal velocities at the lateral model boundaries (left, right, bottom), satisfying a constant bulk extension rate of 10^{-15} s^{-1}. The models were run with a numerical resolution of 150 x 75 m (2000 x 1600 cells) and a Courant number of 0.5 for the adaptive time step (i.e. the maximum displacement per time step is half a grid space). The top of the model is a free surface on which the action of surface processes is not taken into account. The initial thermal field is that of an equilibrium field that includes radiogenic heat production in the continental crust and exhibits 500-550 °C at the Moho. Zero heat flow boundary conditions are prescribed at the lateral sides of the model; the top and bottom boundaries are characterized by a constant temperature (0 and 1330 °C, respectively). The continental crust is initially 30 km thick and is modelled with a visco-plastic layer of moderate strength (anorthite flow law; Rybacki and Dresen, 2004) and includes embedded elliptical bodies of relatively weaker (4 x 67 km ellipses; wet quartzite; Kirby, 1983) and stronger rheologies (4-7 x 42-77 km ellipses; Maryland diabase; Mackwell et al., 1998) representing laterally discontinuous strength variations mimicking structural or lithological heterogeneities. Weak ellipses mimic rheological weak lithologies such as phyllosilicate-rich metasedimentary units in upper and mid-crustal position (e.g. Grosina and the Serie dei Laghi units), whereas strong ellipses stand for rheological strong lithologies such as mid-crustal (Sondalo mafic complex) and lower crustal mafic intrusions (Braccia and Ivrea mafic complexes). The upper subcontinental mantle is initially 40 km thick and is modelled using a visco-plastic layer dominated by dry olivine (Carter and Tsenn, 1987) and incorporates weaker lens-shaped bodies dominated by wet olivine (3 x 61 km ellipses; Carter and Tsenn,

1987) to model heterogeneities in the mantle (e.g. pre-existing petro-fabric, modal variations, crystallized melt pockets). The lower subcontinental mantle is modelled using a purely viscous layer dominated by a wet olivine rheology. No prescribed strain-softening parameterization is applied in the models, the numerical models are hence less prone to mesh-dependence and exhibit a good convergence upon mesh refinement (see Figure S5). The models are also performed using different initial lithospheric structures (see Text S3, Table S4 and Figure S6).

5.1. Modeling results: reference model

The geometrical and rheological evolution of the reference model is depicted in Figs. 7 and 8 (see also Movies S8-S10). Within the first 10% of extension, the deformation of the continental crust is distributed and mainly in the frictional field. The main localizing feature is the weak inclusion originally positioned at about 20 km depth that acts as a *décollement* level in the ductile field (Fig. 8a). The deformation of the upper subcontinental mantle gives rise to an overall necking pattern (Fig. 7b). Some localized deformation occurs close to the Moho where the stronger mantle reaches conditions of frictional deformation and undergoes necking in the regions where heterogeneities induce a local stratification (Fig. 8a). After about 15% of extension, the upper subcontinental mantle is almost totally necked and devoid of any frictional deformation (Fig. 7c, 8b). The activation of numerous frictional shear bands in the crust leads to the formation of a pattern of tilted blocks (Fig. 7c). The stronger heterogeneities present in the crust are still mostly undeformed compared to surrounding material. After 25% of extension, the upper subcontinental mantle is fully necked although the crust in the center of the rift is still about 15 km thick (Fig. 7d). As the initially deep mantle is in direct contact with the crust, the Moho temperature rises to about 600 °C. Frictional deformation is only activated in the crust and occurs on a few shear bands only (Fig. 8c). One frictional structure propagates across the strong central heterogeneity and shears it apart, forming an apparent

large scale pinch and swell structure (Fig. 7d and 8c). The conditions of extreme crustal thinning and final crustal breakup occur after 30% of extension (Fig. 7e). The final necking migrates basinwards (towards the center of the model) due to the presence of the strong central crustal heterogeneity. As the mantle flows closer to the surface, it cools down below 600 °C and reaches the conditions of frictional deformation. As most of the deformation occurs now in the upper subcontinental mantle, the two continental margins do not undergo any further prominent strain (Fig. 8d) while deformation is only accommodated by creep of the lower subcontinental mantle.

5.2. Modeling results: impact of rheological contrasts

The impact of tectonic inheritance is a direct consequence of the strength contrasts between different lithologies. For example, the extension of a small scale multilayer material with negligible strength contrasts may likely not undergo any localized necking (see Schmalholz and Mancktelow, 2016). In order to investigate the impact of strength variations, we systematically increased and decreased the strength contrasts between the crust, mantle and their heterogeneities. To do so, we artificially varied ductile flow strength of the heterogeneities (Fig. 9). Increasing the effective viscosity of weak heterogeneities and reducing the viscosity of strong heterogeneities by a factor of 10 simulated small strength contrasts (Fig. 9a). Conversely, decreasing the viscosity of weak heterogeneities and increasing the viscosity of strong heterogeneities by a factor of 10 simulated large strength contrasts (Fig. 9c). These models were compared to the reference model (Fig. 9b) for similar amounts of extension (40%). The model with low strength contrast clearly differs from the reference model (Fig. 9ab). It is dominated by a distributed thinning of the lithosphere ultimately leading to a single lithosphere-scale necking (Chenin et al., 2018; Fletcher and Hallett, 1983). The model with large strength contrast resembles the reference model but

exhibits much more localized features (Fig. 9bc). The tilted-block pattern in the upper crust is amplified and the overall rift asymmetry is more pronounced.

6. DISCUSSION

The comparison of both field observations from the remnants of the Alpine Tethys and numerical models led to characterize the different structures accommodating the thinning of the continental lithosphere in relation with initial heterogeneities. The detailed comparison between the Alpine Tethys rifted margin architecture based on field observations, the numerical modelling results and related P_0-depth diagrams are provided in Figure S7.

6.1. Distribution of deformation across the rifted margin

6.1.1. The proximal domain

From the proximal to the distal domains, the style of extensional structures significantly changes. In the proximal domain, most of the extension is accommodated by high-angle normal faults essentially developed during the early rifting stage (Fig. 8ab). These faults are generally able to cut across the brittle upper crust before soling into *décollement* levels. Such *décollement* levels may be localized either at the brittle-ductile transition at mid-crustal depth or in weak lithologies (e.g., phyllosilicate-rich layers). In contrast, the deformation of the deepest part of the crust appears to be accommodated by diffuse ductile deformation. At that stage, P_0-depth diagrams are weakly modified (0.32 kbar.km^{-1}) with respect to a normal lithostatic gradient (max. 0.29 kbar.km^{-1}; Fig. 10fg) emphasizing the weak crustal thinning recorded in this domain. This is in agreement with the low accommodation space deduced from the syn- to post-rift sedimentary record (e.g. Eberli, 1988).

6.1.2. The necking zone

The deformation style evolves across the necking zone in association with an increase of crustal thinning. Most of the normal faults affecting the upper crust are progressively rooting on a major *décollement* that can be followed until the development of the proximal domain. At depth, small-scale necking of individual strong layers allows *décollement* levels to connect different crustal levels. Strong layers remain almost undeformed while most of the deformation localizes in surrounding, weak lithologies, conditioning the system for lateral extraction (see section 6.3). In particular the ESZ may represent an example of a *décollement*, delimiting the essentially undeformed Campo unit hosting pre-rift Permian gabbroic intrusions from the overlying, deformed Grosina unit (A-A'). This is similar to lateral variations in lower crustal strain documented in the Southern Alps (Fig. 5). The pre-rift mafic intrusion of the lower crustal IVZ, recorded weak to no rift-related deformation while P_0-depth gradient is almost unmodified with respect to the lithostatic gradient. However, deformation increases in the surrounding metasediments where several rift-related shear zones have been recognized (Figs. 5, 6). The presence of these shear zones is associated with modifications in P_0-depth gradients from 0.42 kbar.km^{-1} close to the main mafic complex in Val Strona (E-E') up to 1.8 kbar.km^{-1} in Val Cannobina (F-F', Fig. 5d). This strain partitioning, both vertically and laterally, is well illustrated in the synthetic P_0-depth diagrams across the necking zone (Fig. 10de) where both the crust and the mantle are characterized by various P_0-depth gradients resulting from the incipient lateral extraction of distinct portions of the continental basement (see section 6.3). As an example, the lower crust in the necking zone may either be weakly deformed, surrounded by high-strain zones with high local P_0-depth gradients (0.43 kbar.km^{-1} to 2.87 kbar.km^{-1}, Fig. 10e) or pervasively deformed with high P_0-depth gradients (1.18 kbar.km^{-1}, Fig. 10d). With more extension, deformation at the surface

starts to be localized along few major detachment faults that remain restricted to the crust whereas the deformation stops in this domain at around 25% (Fig. 8cd).

6.1.3. The distal domain

In the distal domain, highly extended continental crust passes laterally to subcontinental mantle exhumed at the seafloor. Normal faults cutting across the entire residual crust sole into a *décollement* now coinciding with the Moho (Fig. 8ab). Such a configuration has been described in the present-day Iberia margin and identified as the S-reflector (Reston et al., 1996). Deep deformation in this domain is extremely localized: high-strain zones are distributed in initially weak lithologies while strong lithologies remain almost undeformed. Such strain partitioning is explained by the lateral extraction (see section 6.3) of strong layers from the future distal domain during the early extensional stages (Fig. 7). This lateral extraction appears as an efficient process able to thin the continental crust over few kilometers. As this process occurs during extension, local thickening caused by extraction of lateral levels is inhibited. Similar to the continental crust, the mantle is rapidly necked by the interaction of large offset normal faults and *décollement* levels. The direct implication of fully achieved lateral extraction for the associated P_0-depth diagram is the presence of sharp gradients of P_0 with depth surrounding preserved domains (0.42 kbar.km^{-1}, Fig. 10c). This is also reported for the two distal margin examples in the Eastern Alps (Fig. 3). In the southern distal margin (C-C'), the pre-rift upper and lower crusts are juxtaposed via the Margna shear zone (Figs. 3, 4ef). In this context, the Margna shear zone represents an extraction fault that remains after the extraction of mid-crustal units. Eventually, deformation localizes along main detachment faults with increasing strain amount to finally exhume at the seafloor deep levels such as the mantle (Figs. 7, 8).

6.2. The role of heterogeneities

Our observations and numerical models indicate that initial mechanical heterogeneities have a first-order control on the mechanisms of thinning and eventually on the evolution and architecture of rifted margins. Among others, the relative strength contrasts between the heterogeneities and their initial position in the continental lithosphere are key parameters.

For small rheological contrasts (effective viscosity contrast decreased by a factor of 10; see Table S4 for reference rheological parameters), deformation is highly distributed over the entire section (Fig. 9) and the necking of both the mantle and the crust are symmetrical. This setting leads to the formation of a wide zone of lithospheric thinning, delaying or even inhibiting mantle exhumation. In contrast, moderate and large strength contrasts (reference model or effective viscosity contrast increased by a factor of 10) rapidly partition the deformation in weak lithologies: decoupling levels may be active over large distances across the margin and their lifetime may also be protracted. Strain partitioning triggers the lateral extraction of the strong parts of the crust or mantle that remains weakly deformed to undeformed. The removal of the strong layers permits the connection of weak layers by extensional structures leading to the mechanical coupling of the crust and the mantle and permits exhumation of the latter to the seafloor. Our model does not integrate decompression melting which, if arriving early enough with respect to crustal thinning, may abort mantle exhumation at the seafloor (Davis and Lavier, 2017; Larsen et al., 2018; Ros et al., 2017; Tugend et al., 2018). In general, significant rheological contrasts favour mantle exhumation and less total strain is requested (Fig. 9). Finally, the detachment fault responsible for exhumation generates a margin asymmetry.

The initial vertical and horizontal position of heterogeneities also has implications for the distribution of the extensional deformation (see also Figure S6). At the lithospheric scale, the role of heterogeneities seems to be negligible at the shallowest levels; high-angle brittle

structures are generated independent of the position of heterogeneities but may still be locally controlled by inherited structures. Upper crustal heterogeneities are therefore behaving as passive markers of the deformation. In contrast, the development of deep deformation bands in the ductile regime is strongly controlled (in case of sufficient strength contrast) by the presence of weak lithologies localizing the deformation or strong lithologies forcing deformation either to shallower or deeper levels. This is notably the case for *décollement* levels onto which normal faults sole.

From both field observations and numerical models, we show that at the scale of the lithosphere, deformation is preferentially localized in initially weak lithologies, affecting to a lesser extent initially strong lithologies (see Figure S7). The most important parameter is the rheological contrast between two lithologies and not their absolute rheological parameters (e.g. Handy, 1994). Examples for weak lithologies could be phyllosilicate-rich (meta-) sediments with a pre-rift foliation (Shea and Kronenberg, 1993) or granitoids while strong lithologies could be mafic intrusions. The necking zone of the Eastern Alps best exemplifies this relation: the Grosina unit, which is made of metasediment and orthogneiss derived from granitoid, localizes several rift-related structures, whereas the underlying Sondalo gabbroic complex and surrounding Campo unit escaped rift-related deformation. Granitoids may even be the weakest lithologies in case of a more mafic continental crust. Once rifting is initiated, several mechanisms may further enhance weakening of the deforming zone by grain size reduction (Fitz Gerald and Stünitz, 1993; Handy, 1990), metamorphic retrogression (Wintsch et al., 1995), shear heating (Brun and Cobbold, 1980) or formation of petrofabric (Holyoke and Tullis, 2006).

6.3. The importance of heterogeneity-enhanced extraction tectonics

The incorporation of heterogeneities highlights that extraction tectonics represent an efficient manner to accommodate lithospheric thinning. As exemplified by Froitzheim et al.

(2006), it requires to localize the deformation in conjugate shear zones surrounding an undeformed to weakly deformed volume. Shear zones have opposite sense of displacement and are connected at the tip of the volume, leaving an extraction fault or shear zone behind (see Fig. 1 of Froitzheim et al., 2006). In extensional tectonic systems, this extraction fault may record a complex sense of motion and amount of strain (Froitzheim et al., 2006). Such mechanisms have been proposed to exist in the extending continental lithosphere, either in late- to post-orogenic systems (Fossen et al., 2014) or during the formation of extremely extended margins (Clerc and Lagabrielle, 2014; Froitzheim et al., 2006; Mohn et al., 2012).

Lateral extraction is thus a viable mechanism only in case of depth-dependent thinning, likely activated if kilometre-scale, laterally discontinuous heterogeneities are present. In the models (Figs. 7-10), the heterogeneities pre-set the system to enhance extraction. However, lateral discontinuity can also be generated during extension. As shown by Brun and Beslier (1996) and Duretz et al. (2016b), initially strong and continuous layers may be necked to form individual large-scale boudins that are conducive to extraction by continuous extension.

Field examples of this necking-related mechanism are well documented in the Eastern Alps. Whereas distal-most domains are showing examples in which extraction has been completed, aborted extraction can be seen in the necking zone (Figs. 3, 5). Indeed, the ESZ affects the orthogneissic Grosina unit, leaving undeformed the underlying Campo unit, which hosts a Permian gabbro inhibiting deformation in the latter unit. Such observations show the control of pre-existing lithologies on the partitioning of deformation and led to the selection of different extraction levels during rifting. Hence, the finite result of extreme lithospheric thinning is the juxtaposition of internally weakly to undeformed sections of the continental lithosphere. These sections are juxtaposed across complex extensional high-strain zones that act either as decoupling horizons with relatively horizontal geometries or variably inclined

519 structures. Such processes explain the preservation of pre-rift fabric and lithology in
520 extremely thinned continental crust.

521 **6.4 Implications for present-day rifted margins**

522 This study suggests that, at least locally, the discrepancy between recognized faulting
523 and observed total crustal thinning is the result of a complex interplay between intra-basement
524 deformation zones. Several contributions have already emphasized the role of boudinage in
525 present-day margins as for instance documented offshore Britain (Reston, 1988). Our results
526 further explain the composition of extremely thinned distal domains; depending on the initial
527 architecture of continental lithosphere, various crustal levels can be extracted from the future
528 distal domain. This domain may therefore be composed of a juxtaposition of different crustal
529 levels with different pre-rift and syn-rift *P-T* histories. As consequence even in the most distal
530 margins, undeformed pre-rift crustal levels can therefore be preserved, surrounded by rift-
531 related extensional structures. In the Iberia-Newfoundland rifted margin, the distal domain
532 was interpreted to be the result of the juxtaposition of both upper and lower crust inferred
533 from both drilling results and seismic surveys (e.g. Péron-Pinvidic and Manatschal, 2009). In
534 contrast, the exhumation of the lower crust was proposed in parts of the SW Barents sea
535 (Gernigon et al., 2014), the Gulf of Lion (Jolivet et al., 2015) or offshore Gabon (Clerc et al.,
536 2018).

537 **7. CONCLUSION**

538 We investigated the control of initial mechanical heterogeneities such as changing
539 lithologies, inherited mechanical anisotropies (e.g., rock fabrics) or pre-rift structures on the
540 rifting kinematics and dynamics.

541 The pre-rift architecture of the continental lithosphere was reconstructed from field
542 observations in the remnants of the Alpine Tethys. The evolution of the different portions of

543 the continental lithosphere was tracked during the rifting by studying initial pressure (P_0) –
544 depth diagrams highlighting the homogenous thinning or missing distinct pre-rift levels of the
545 lithosphere.

546 We compared these observations to two-dimensional thermo-mechanical numerical
547 models investigating the role of initial lithospheric heterogeneities for the architecture and
548 evolution of rifted margins. The style of lithospheric extension is strongly influenced by the
549 rheological contrasts between the embedded heterogeneities within the continental crust /
550 lithosphere.

551 These multidisciplinary approaches emphasized the critical role of extraction tectonics
552 that appears as an efficient mechanism to thin the continental lithosphere. Such mechanism
553 initiates in the necking zone, recording strong variations in strain distribution, both vertically
554 and horizontally. As a consequence, the deep deformation in the distal domain is localized
555 along high-strain zones left behind after extraction of various strong levels. Depending on the
556 initial position of the heterogeneities, different levels may be selected for lateral extraction
557 during rifting, explaining the variable composition of distal margin basement.

558 **ACKNOWLEDGMENT**

559 The authors thank Antonio Langone, Gianreto Manatschal, Patricio Figueredo and
560 Christopher Johnson for discussions as well as Lin Chen and an anonymous referee for their
561 reviews. This work is dedicated to Marco Beltrando.

562 **FUNDING**

563 This work was supported by the University of Lausanne and an ExxonMobil research
564 grant to BP and OM.

SUPPORTING INFORMATION

Supplementary material 1

Table S1. Compilation of published *P-T-t* estimates from the Eastern Alps

Table S2. Compilation of published *P-T-t* estimates from the Southern Alps and associated statistics

Text S3. Modelling methodology and parameters

Table S4. Summary of thermal and rheological parameters used in the numerical experiments

Figure S5. Model resolution tests

Figure S6. Additional numerical models

Figure S7. P_0-depth summary figure

Supplementary material 2

Movie S8. Reference model with phase coloring

Supplementary material 3

Movie S9. Accumulated strain of the reference model

Supplementary material 4

Movie S10. Frictional and ductile strain rate of the reference model

REFERENCES

Altenberger, U., 1997. Strain localization mechanisms in deep-seated layered rocks. Geol. Rundschau 86, 56–68. doi:10.1007/s005310050121

Beltrando, M., Compagnoni, R., Ferrando, S., Mohn, G., Frasca, G., Odasso, N., Vokmanovič, Z., Masini, E., 2015a. Crustal thinning and mantle exhumation in the Levone area (Southern Canavese Zone, Western Alps), in: A Field Guide Across the Margins of Alpine Tethys, J. Virtual Explor., Vol. 48, Edited by G. Manatscal et Al. doi:10.3809/jvirtex.2013.00326.

Beltrando, M., Manatschal, G., Mohn, G., Dal Piaz, G. V, Vitale Brovarone, A., Masini, E., 2014. Recognizing remnants of magma-poor rifted margins in high-pressure orogenic belts: The Alpine case study. Earth-Science Rev. 131, 88–115. doi:10.1016/J.EARSCIREV.2014.01.001

Beltrando, M., Stockli, D.F., Decarlis, A., Manatschal, G., 2015b. A crustal-scale view at rift localization along the fossil Adriatic margin of the Alpine Tethys preserved in NW Italy. Tectonics 34, 1927–1951. doi:10.1002/2015TC003973

Beltrando, M., Zibra, I., Montanini, A., Tribuzio, R., 2013. Crustal thinning and exhumation along a fossil magma-poor distal margin preserved in Corsica: A hot rift to drift transition? Lithos 168–169, 99–112. doi:http://dx.doi.org/10.1016/j.lithos.2013.01.017

Bertotti, G., Picotti, V., Bernoulli, D., Castellarin, A., 1993. From rifting to drifting: tectonic evolution of the South-Alpine upper crust from the Triassic to the Early Cretaceous. Sediment. Geol. 86, 53–76. doi:http://dx.doi.org/10.1016/0037-0738(93)90133-P

Bissig, T., Hermann, J., 1999. From pre-Alpine extension to Alpine convergence: the example of the southwestern margin of the Margna nappe (Val Malenco, N-Italy). Schweizerische Mineral. und Petrogr. Mitteilungen 79, 363–380.

Brodie, K.H., Rex, D., Rutter, E.H., 1989. On the age of deep crustal extensional faulting in the Ivrea zone, northern Italy. Geol. Soc. London, Spec. Publ. 45, 203–210.

Brun, J.P., Beslier, M.O., 1996. Mantle exhumation at passive margins. Earth Planet. Sci. Lett. 142, 161–173. doi:http://dx.doi.org/10.1016/0012-821X(96)00080-5

Brun, J.P., Cobbold, P.R., 1980. Strain heating and thermal softening in continental shear zones: a review. J. Struct. Geol. 2, 149–158. doi:10.1016/0191-8141(80)90045-0

Büchi, H., 1994. Der variskiscke Magmatismus in der östlichen Bernina. Schweizerische Mineral. und Petrogr. Mitteilungen 74, 359–371.

Carter, N.L., Tsenn, M.C., 1987. Flow properties of continental lithosphere. Tectonophysics 136, 27–63. doi:https://doi.org/10.1016/0040-1951(87)90333-7

Clerc, C., Jolivet, L., Ringenbach, J.-C., 2015. Ductile extensional shear zones in the lower crust of a passive margin. Earth Planet. Sci. Lett. 431, 1–7. doi:http://dx.doi.org/10.1016/j.epsl.2015.08.038

Clerc, C., Lagabrielle, Y., 2014. Thermal control on the modes of crustal thinning leading to mantle exhumation: Insights from the Cretaceous Pyrenean hot paleomargins. Tectonics 33, 1340–1359.

Clerc, C., Ringenbach, J.-C., Jolivet, L., Ballard, J.-F., 2018. Rifted margins: Ductile deformation, boudinage, continentward-dipping normal faults and the role of the weak lower crust. Gondwana Res. 53, 20–40. doi:https://doi.org/10.1016/j.gr.2017.04.030

Chenin, P., Schmalholz, S.M., Manatschal, G., Karner, G.D., 2018. Necking of the Lithosphere: A Reappraisal of Basic Concepts With Thermo-Mechanical Numerical Modeling. J. Geophys. Res. Solid Earth 123, 5279–5299. doi:10.1029/2017JB014155

Davis, J.K., Lavier, L.L., 2017. Influences on the development of volcanic and magma-poor morphologies during passive continental rifting. Geosphere 13, 1524–1540. doi:10.1130/GES01538.1

630 Decarlis, A., Beltrando, M., Manatschal, G., Ferrando, S., Carosi, R., 2017. Architecture of
631 the Distal Piedmont-Ligurian Rifted Margin in NW Italy: Hints for a Flip of the Rift
632 System Polarity. Tectonics 36, 2388–2406. doi:10.1002/2017TC004561
633 Demarchi, G., Quick, J.E., Sinigoi, S., Mayer, A., 1998. Pressure gradient and original
634 orientation of a lower-crustal intrusion in the Ivrea-Verbano zone, Northern Italy. J.
635 Geol. 106, 609–622.
636 Dewey, J.F., Bird, J.M., 1970. Mountain belts and the new global tectonics. J. Geophys. Res.
637 75, 2625–2647. doi:10.1029/JB075i014p02625
638 Duretz, T., May, D.A., Yamato, P., 2016a. A free surface capturing discretization for the
639 staggered grid finite difference scheme. Geophys. J. Int. 204, 1518–1530.
640 Duretz, T., Petri, B., Mohn, G., Schmalholz, S.M., Schenker, F.L., Müntener, O., 2016b. The
641 importance of structural softening for the evolution and architecture of passive margins.
642 Sci. Rep. 6, 38704. doi:10.1038/srep38704
643 Eberli, G.P., 1988. The evolution of the southern continental margin of the Jurassic Tethys
644 Ocean as recorded in the Allgäu Formation of the Austroalpine Nappes of Graubünden
645 (Switzerland). Eclogae Geol. Helv. 81, 175–214.
646 Epin, M.-E., Manatschal, G., Amann, M., 2017. Defining diagnostic criteria to describe the
647 role of rift inheritance in collisional orogens: the case of the Err-Platta nappes
648 (Switzerland). Swiss J. Geosci. 110, 419–438. doi:10.1007/s00015-017-0271-6
649 Ferrando, S., Bernoulli, D., Compagnoni, R., 2004. The Canavese zone (internal Western
650 Alps): a distal margin of Adria. Schweizerische Mineral. und Petrogr. Mitteilungen 84,
651 237–256.
652 Fitz Gerald, J.D., Stünitz, H., 1993. Deformation of granitoids at low metamorphic grade. I:
653 Reactions and grain size reduction. Tectonophysics 221, 269–297. doi:10.1016/0040-
654 1951(93)90163-E
655 Fletcher, R.C., Hallet, B., 1983. Unstable extension of the lithosphere: A mechanical model
656 for basin-and-range structure. J. Geophys. Res. Solid Earth 88, 7457–7466.
657 doi:10.1029/JB088iB09p07457
658 Fossen, H., Gabrielsen, R.H., Faleide, J.I., Hurich, C.A., 2014. Crustal stretching in the
659 Scandinavian Caledonides as revealed by deep seismic data. Geol. .
660 Fountain, D.M., Salisbury, M.H., 1981. Exposed cross-sections through the continental crust:
661 implications for crustal structure, petrology, and evolution. Earth Planet. Sci. Lett. 56,
662 263–277. doi:http://dx.doi.org/10.1016/0012-821X(81)90133-3
663 Frasca, G., Gueydan, F., Brun, J.-P., Monié, P., 2016. Deformation mechanisms in a
664 continental rift up to mantle exhumation. Field evidence from the western Betics, Spain.
665 Mar. Pet. Geol. 76, 310–328. doi:http://dx.doi.org/10.1016/j.marpetgeo.2016.04.020
666 Froitzheim, N., Eberli, G.P., 1990. Extensional detachment faulting in the evolution of a
667 Tethys passive continental margin, Eastern Alps, Switzerland. Geol. Soc. Am. Bull. 102,
668 1297–1308. doi:10.1130/0016-7606(1990)102<1297:edfite>2.3.co;2
669 Froitzheim, N., Pleuger, J., Nagel, T.J., 2006. Extraction faults. J. Struct. Geol. 28, 1388–
670 1395. doi:https://doi.org/10.1016/j.jsg.2006.05.002
671 Froitzheim, N., Schmid, S.M., Conti, P., 1994. Repeated change from crustal shortening to
672 orogen-parallel extension in the Austroalpine units of Graubünden. Eclogae Geol. Helv.
673 87, 559–612.
674 Gernigon, L., Brönner, M., Roberts, D., Olesen, O., Nasuti, A., Yamasaki, T., 2014. Crustal
675 and basin evolution of the southwestern Barents Sea: From Caledonian orogeny to
676 continental breakup. Tectonics 33, 347–373. doi:10.1002/2013TC003439
677 Gerya, T. V, Yuen, D.A., 2003. Characteristics-based marker-in-cell method with
678 conservative finite-differences schemes for modeling geological flows with strongly
679 variable transport properties. Phys. Earth Planet. Inter. 140, 293–318.

680 doi:https://doi.org/10.1016/j.pepi.2003.09.006
681 Handy, M.R., 1987. The structure, age and kinematics of the Pogallo Fault Zone; Southern
682 Alps, northwestern Italy. Eclogae Geol. Helv. 80, 595–632.
683 Handy, M.R., 1990. The solid-state flow of polymineralic rocks. J. Geophys. Res. 95, 8647.
684 doi:10.1029/JB095iB06p08647
685 Handy, M.R., 1994. Flow laws for rocks containing two non-linear viscous phases: A
686 phenomenological approach. J. Struct. Geol. 16, 287–301. doi:10.1016/0191-
687 8141(94)90035-3
688 Handy, M.R., Franz, L., Heller, F., Janott, B., Zurbriggen, R., 1999. Multistage accretion and
689 exhumation of the continental crust (Ivrea crustal section, Italy and Switzerland).
690 Tectonics 18, 1154–1177. doi:10.1029/1999tc900034
691 Hansmann, W., Müntener, O., Hermann, J., 2001. U-Pb zircon geochronology of a tholeiitic
692 intrusion and associated migmatites at a continental crust-mantle transition, Val
693 Malenco, Italy. Schweizerische Mineral. und Petrogr. Mitteilungen 81, 239–255.
694 Henk, A., Franz, L., Teufel, S., Oncken, O., 1997. Magmatic underplating, extension, and
695 crustal reeguilibration: insights from a cross-section through the Ivrea Zone and Strona-
696 Ceneri Zone, Northern Italy. J. Geol. 105, 367–377.
697 Hermann, J., Müntener, O., 1996. Extension-related structures in the Malenco-Margna-
698 system: implications for paleogeography and consequences for rifting and Alpine
699 tectonics. Schweizerische Mineral. und Petrogr. Mitteilungen 76, 501–519.
700 Holyoke, C.W., Tullis, J., 2006. Mechanisms of weak phase interconnection and the effects of
701 phase strength contrast on fabric development. J. Struct. Geol. 28, 621–640.
702 doi:10.1016/j.jsg.2006.01.008
703 Huismans, R.S., Beaumont, C., 2014. Rifted continental margins: The case for depth-
704 dependent extension. Earth Planet. Sci. Lett. 407, 148–162.
705 doi:https://doi.org/10.1016/j.epsl.2014.09.032
706 Jolivet, L., Gorini, C., Smit, J., Leroy, S., 2015. Continental breakup and the dynamics of
707 rifting in back-arc basins: The Gulf of Lion margin. Tectonics 34, 662–679.
708 doi:10.1002/2014TC003570
709 Karner, G.D., Driscoll, N.W., Barker, D.H.N., 2003. Syn-rift regional subsidence across the
710 West African continental margin: the role of lower plate ductile extension. Geol. Soc.
711 London, Spec. Publ. 207, 105 LP-129.
712 Kenkmann, T., Dresen, G., 2002. Dislocation microstructure and phase distribution in a lower
713 crustal shear zone – an example from the Ivrea-Zone, Italy. Int. J. Earth Sci. 91, 445–
714 458. doi:10.1007/s00531-001-0236-9
715 Kirby, S.H., 1983. Rheology of the lithosphere. Rev. Geophys. 21, 1458–1487.
716 doi:10.1029/RG021i006p01458
717 Kusznir, N.J., Karner, G.D., 2007. Continental lithospheric thinning and breakup in response
718 to upwelling divergent mantle flow: application to the Woodlark, Newfoundland and
719 Iberia margins. Geol. Soc. London, Spec. Publ. 282, 389 LP-419.
720 Langone, A., Padrón-Navarta José, A., Ji, W.-Q., Zanetti, A., Mazzucchelli, M., Tiepolo, M.,
721 Giovanardi, T., Bonazzi, M., 2017. Ductile–brittle deformation effects on crystal-
722 chemistry and U–Pb ages of magmatic and metasomatic zircons from a dyke of the
723 Finero Mafic Complex (Ivrea–Verbano Zone, Italian Alps). Lithos 284–285, 493–511.
724 doi:https://doi.org/10.1016/j.lithos.2017.04.020
725 Langone, A., Zanetti, A., Daczko, N.R., Piazolo, S., Tiepolo, M., Mazzucchelli, M., 2018.
726 Zircon U–Pb dating of a lower crustal shear zone: a case study from the northern sector
727 of the Ivrea-Verbano Zone (Val Cannobina, Italy). Tectonics n/a-n/a.
728 doi:10.1002/2017TC004638
729 Larsen, H.C., Mohn, G., Nirrengarten, M., Sun, Z., Stock, J., Jian, Z., Klaus, A., Alvarez-

730 Zarikian, C.A., Boaga, J., Bowden, S.A., Briais, A., Chen, Y., Cukur, D., Dadd, K.,
731 Ding, W., Dorais, M., Ferré, E.C., Ferreira, F., Furusawa, A., Gewecke, A., Hinojosa, J.,
732 Höfig, T.W., Hsiung, K.H., Huang, B., Huang, E., Huang, X.L., Jiang, S., Jin, H.,
733 Johnson, B.G., Kurzawski, R.M., Lei, C., Li, B., Li, L., Li, Y., Lin, J., Liu, C., Liu, C.,
734 Liu, Z., Luna, A.J., Lupi, C., McCarthy, A., Ningthoujam, L., Osono, N., Peate, D.W.,
735 Persaud, P., Qiu, N., Robinson, C., Satolli, S., Sauermilch, I., Schindlbeck, J.C., Skinner,
736 S., Straub, S., Su, X., Su, C., Tian, L., van der Zwan, F.M., Wan, S., Wu, H., Xiang, R.,
737 Yadav, R., Yi, L., Yu, P.S., Zhang, C., Zhang, J., Zhang, Y., Zhao, N., Zhong, G.,
738 Zhong, L., 2018. Rapid transition from continental breakup to igneous oceanic crust in
739 the South China Sea. Nat. Geosci. 11, 782–789. doi:10.1038/s41561-018-0198-1
740 Mackwell, S.J., Zimmerman, M.E., Kohlstedt, D.L., 1998. High- temperature deformation of
741 dry diabase with application to tectonics on Venus. J. Geophys. Res. Solid Earth 103,
742 975–984. doi:10.1029/97JB02671
743 Manatschal, G., Lavier, L., Chenin, P., 2015. The role of inheritance in structuring
744 hyperextended rift systems: Some considerations based on observations and numerical
745 modeling. Gondwana Res. 27, 140–164. doi:http://dx.doi.org/10.1016/j.gr.2014.08.006
746 Manatschal, G., Nievergelt, P., 1997. A continent-ocean transition recorded in the Err and
747 Platta nappes (Eastern Switzerland). Eclogae Geol. Helv. 90, 3–27.
748 Masini, E., Manatschal, G., Mohn, G., Ghienne, J.-F., Lafont, F., 2011. The tectono-
749 sedimentary evolution of a supra-detachment rift basin at a deep-water magma-poor
750 rifted margin: the example of the Samedan Basin preserved in the Err nappe in SE
751 Switzerland. Basin Res. 23, 652–677. doi:10.1111/j.1365-2117.2011.00509.x
752 Mohn, G., Manatschal, G., Beltrando, M., Masini, E., Kusznir, N., 2012. Necking of
753 continental crust in magma-poor rifted margins: Evidence from the fossil Alpine Tethys
754 margins. Tectonics 31, 1–28.
755 Mohn, G., Manatschal, G., Masini, E., Müntener, O., 2011. Rift-related inheritance in
756 orogens: a case study from the Austroalpine nappes in Central Alps (SE-Switzerland and
757 N-Italy). Int. J. Earth Sci. 100, 937–961. doi:10.1007/s00531-010-0630-2
758 Mohn, G., Manatschal, G., Müntener, O., Beltrando, M., Masini, E., 2010. Unravelling the
759 interaction between tectonic and sedimentary processes during lithospheric thinning in
760 the Alpine Tethys margins. Int. J. Earth Sci. 99, 75–101. doi:10.1007/s00531-010-0566-
761 6
762 Mulch, A., Cosca, M., Handy, M., 2002a. In-situ UV-laser 40Ar/39Ar geochronology of a
763 micaceous mylonite : an example of defect-enhanced argon loss. Contrib. to Mineral.
764 Petrol. 142, 738–752. doi:10.1007/s00410-001-0325-6
765 Mulch, A., Rosenau, M., Dörr, W., Handy, M., 2002b. The age and structure of dikes along
766 the tectonic contact of the Ivrea-Verbano and Strona-Ceneri Zones (southern Alps,
767 Northern Italy, Switzerland). Schweizerische Mineral. und Petrogr. Mitteilungen 82, 55–
768 76.
769 Müntener, O., Hermann, J., 2001. The role of lower crust and continental upper mantle during
770 formation of non-volcanic passive margins: evidence from the Alps. Geol. Soc. London,
771 Spec. Publ. 187, 267–288. doi:10.1144/gsl.sp.2001.187.01.13
772 Müntener, O., Hermann, J., Trommsdorff, V., 2000. Cooling History and Exhumation of
773 Lower-Crustal Granulite and Upper Mantle (Malenco, Eastern Central Alps). J. Petrol.
774 41, 175–200. doi:10.1093/petrology/41.2.175
775 Müntener, O., Manatschal, G., Desmurs, L., Pettke, T., 2010. Plagioclase Peridotites in
776 Ocean–Continent Transitions: Refertilized Mantle Domains Generated by Melt
777 Stagnation in the Shallow Mantle Lithosphere. J. Petrol. 51, 255–294.
778 doi:10.1093/petrology/egp087
779 Osmundsen, P.T., Ebbing, J., 2008. Styles of extension offshore mid-Norway and

780 implications for mechanisms of crustal thinning at passive margins. Tectonics 27, 1–25.
781 doi:10.1029/2007TC002242
782 Péron-Pinvidic, G., Manatschal, G., 2009. The final rifting evolution at deep magma-poor
783 passive margins from Iberia-Newfoundland: a new point of view. Int. J. Earth Sci. 98,
784 1581–1597. doi:10.1007/s00531-008-0337-9
785 Petri, B., Mohn, G., Skrzypek, E., Mateeva, T., Galster, F., Manatschal, G., 2017. U–Pb
786 geochronology of the Sondalo gabbroic complex (Central Alps) and its position within
787 the Permian post-Variscan extension. Int. J. Earth Sci. 106, 2873–2893.
788 doi:10.1007/s00531-017-1465-x
789 Petri, B., Mohn, G., Štípská, P., Schulmann, K., Manatschal, G., 2016. The Sondalo gabbro
790 contact aureole (Campo unit, Eastern Alps): implications for mid-crustal mafic magma
791 emplacement. Contrib. to Mineral. Petrol. 171, 52. doi:10.1007/s00410-016-1263-7
792 Petri, B., Skrzypek, E., Mohn, G., Mateeva, T., Robion, P., Schulmann, K., Manatschal, G.,
793 Müntener, O., 2018. Mechanical anisotropies and mechanisms of mafic magma ascent in
794 the middle continental crust: The Sondalo magmatic system (N Italy). GSA Bull. 130,
795 331–352. doi:10.1130/B31693.1
796 Popov, A.A., Sobolev, S. V, 2008. SLIM3D: A tool for three-dimensional thermomechanical
797 modeling of lithospheric deformation with elasto-visco-plastic rheology. Phys. Earth
798 Planet. Inter. 171, 55–75. doi:https://doi.org/10.1016/j.pepi.2008.03.007
799 Quick, J.E., Sinigoi, S., Snoke, A.W., Kalakay, T.J., Mayer, A., Peressini, G., 2003. Geologic
800 map of the southern Ivrea-Verbano Zone, northwestern Italy: U.S. Geological Survey
801 Geologic Investigations Series Map I-2776, scale 1:25,000 22 p.
802 Rader, E., Emry, E., Schmerr, N., Frost, D., Cheng, C., Menard, J., Yu, C.-Q., Geist, D., 2015.
803 Characterization and Petrological Constraints of the Midlithospheric Discontinuity.
804 Geochemistry, Geophys. Geosystems 16, 3484–3504. doi:10.1002/2015GC005943
805 Reston, T., 2007a. Extension discrepancy at North Atlantic nonvolcanic rifted margins:
806 Depth-dependent stretching or unrecognized faulting? Geology 35, 367–370.
807 Reston, T., 2007b. The formation of non-volcanic rifted margins by the progressive extension
808 of the lithosphere: the example of the West Iberian margin. Geol. Soc. London, Spec.
809 Publ. 282, 77 LP-110.
810 Reston, T.J., 1988. Evidence for shear zones in the lower crust offshore Britain. Tectonics 7,
811 929–945. doi:10.1029/TC007i005p00929
812 Reston, T.J., Krawczyk, C.M., Klaeschen, D., 1996. The S reflector west of Galicia (Spain):
813 Evidence from prestack depth migration for detachment faulting during continental
814 breakup. J. Geophys. Res. Solid Earth 101, 8075–8091. doi:10.1029/95JB03466
815 Ros, E., Pérez-Gussinyé, M., Araújo, M., Thoaldo Romeiro, M., Andrés-Martínez, M.,
816 Morgan, J.P., 2017. Lower Crustal Strength Controls on Melting and Serpentinization at
817 Magma-Poor Margins: Potential Implications for the South Atlantic. Geochemistry,
818 Geophys. Geosystems 18, 4538–4557. doi:10.1002/2017GC007212
819 Rybacki, E., Dresen, G., 2004. Deformation mechanism maps for feldspar rocks.
820 Tectonophysics 382, 173–187. doi:https://doi.org/10.1016/j.tecto.2004.01.006
821 Schmalholz, S.M., Duretz, T., 2017. Impact of grain size evolution on necking in calcite
822 layers deforming by combined diffusion and dislocation creep. J. Struct. Geol. 103, 37–
823 56. doi:https://doi.org/10.1016/j.jsg.2017.08.007
824 Schmalholz, S.M., Mancktelow, N.S., 2016. Folding and necking across the scales: a review
825 of theoretical and experimental results and their applications. Solid Earth 7, 1417–1465.
826 doi:10.5194/se-7-1417-2016
827 Schmid, S.M., Zingg, A., Handy, M., 1987. The kinematics of movements along the Insubric
828 Line and the emplacement of the Ivrea Zone. Tectonophysics 135, 47–66.
829 doi:http://dx.doi.org/10.1016/0040-1951(87)90151-X

Schuster, R., Stüwe, K., 2008. Permian metamorphic event in the Alps. Geology 36, 603–606. doi:10.1130/G24703A.1

Shea, W.T., Kronenberg, A.K., 1993. Strength and anisotropy of foliated rocks with varied mica contents. J. Struct. Geol. 15, 1097–1121. doi:https://doi.org/10.1016/0191-8141(93)90158-7

Siegesmund, S., Layer, P., Dunkl, I., Vollbrecht, A., Steenken, A., Wemmer, K., Ahrendt, H., 2008. Exhumation and deformation history of the lower crustal section of the Valstrona di Omegna in the Ivrea Zone, southern Alps. Geol. Soc. London, Spec. Publ. 298, 45–68. doi:10.1144/sp298.3

Spalla, M.I., Zanoni, D., Marotta, A.M., Rebay, G., Roda, M., Zucali, M., Gosso, G., 2014. The transition from Variscan collision to continental break-up in the Alps: insights from the comparison between natural data and numerical model predictions. Geol. Soc. London, Spec. Publ. 405. doi:10.1144/sp405.11

Thybo, H., Artemieva, I.M., 2013. Moho and magmatic underplating in continental lithosphere. Tectonophysics 609, 605–619. doi:http://dx.doi.org/10.1016/j.tecto.2013.05.032

Tugend, J., Gillard, M., Manatschal, G., Nirrengarten, M., Harkin, C., Epin, M.-E., Sauter, D., Autin, J., Kusznir, N., McDermott, K., 2018. Reappraisal of the magma-rich versus magma-poor rifted margin archetypes. Geol. Soc. London, Spec. Publ. 476, SP476.9. doi:10.1144/SP476.9

Tommasi, A., Vauchez, A., 2001. Continental rifting parallel to ancient collisional belts: an effect of the mechanical anisotropy of the lithospheric mantle. Earth Planet. Sci. Lett. 185, 199–210. doi:https://doi.org/10.1016/S0012-821X(00)00350-2

Von Quadt, A., Grünenfelder, M., Büchi, H., 1994. U-Pb zircon ages from igneous rocks of the Bernina nappe system (Grisons, Switzerland). Schweizerische Mineral. und Petrogr. Mitteilungen 74, 373–382.

von Raumer, J.F., Bussy, F., Schaltegger, U., Schulz, B., Stampfli, G.M., 2013. Pre-Mesozoic Alpine basements—Their place in the European Paleozoic framework. Geol. Soc. Am. Bull. 125, 89–108.

Whitmarsh, R.B., Dean, S.M., Minshull, T.A., Tompkins, M., 2000. Tectonic implications of exposure of lower continental crust beneath the Iberia Abyssal Plain, Northeast Atlantic Ocean: Geophysical evidence. Tectonics 19, 919–942. doi:10.1029/2000TC900016

Wintsch, R.P., Christoffersen, R., Kronenberg, A.K., 1995. Fluid-rock reaction weakening of fault zones. J. Geophys. Res. Solid Earth 100, 13021–13032. doi:10.1029/94JB02622

Wolff, R., Dunkl, I., Kiesselbach, G., Wemmer, K., Siegesmund, S., 2012. Thermochronological constraints on the multiphase exhumation history of the Ivrea-Verbano Zone of the Southern Alps. Tectonophysics 579, 104–117. doi:http://dx.doi.org/10.1016/j.tecto.2012.03.019

Zastrozhnov, D., Gernigon, L., Gogin, I., Abdelmalak, M.M., Planke, S., Faleide, J.I., Eide, S., Myklebust, R., 2018. Cretaceous-Paleocene Evolution and Crustal Structure of the Northern Vøring Margin (Offshore Mid-Norway): Results from Integrated Geological and Geophysical Study. Tectonics. doi:10.1002/2017TC004655

Zingg, A., Handy, M.R., Hunziker, J.C., Schmid, S.M., 1990. Tectonometamorphic history of the Ivrea Zone and its relationship to the crustal evolution of the Southern Alps. Tectonophysics 182, 169–192. doi:http://dx.doi.org/10.1016/0040-1951(90)90349-D

FIGURES

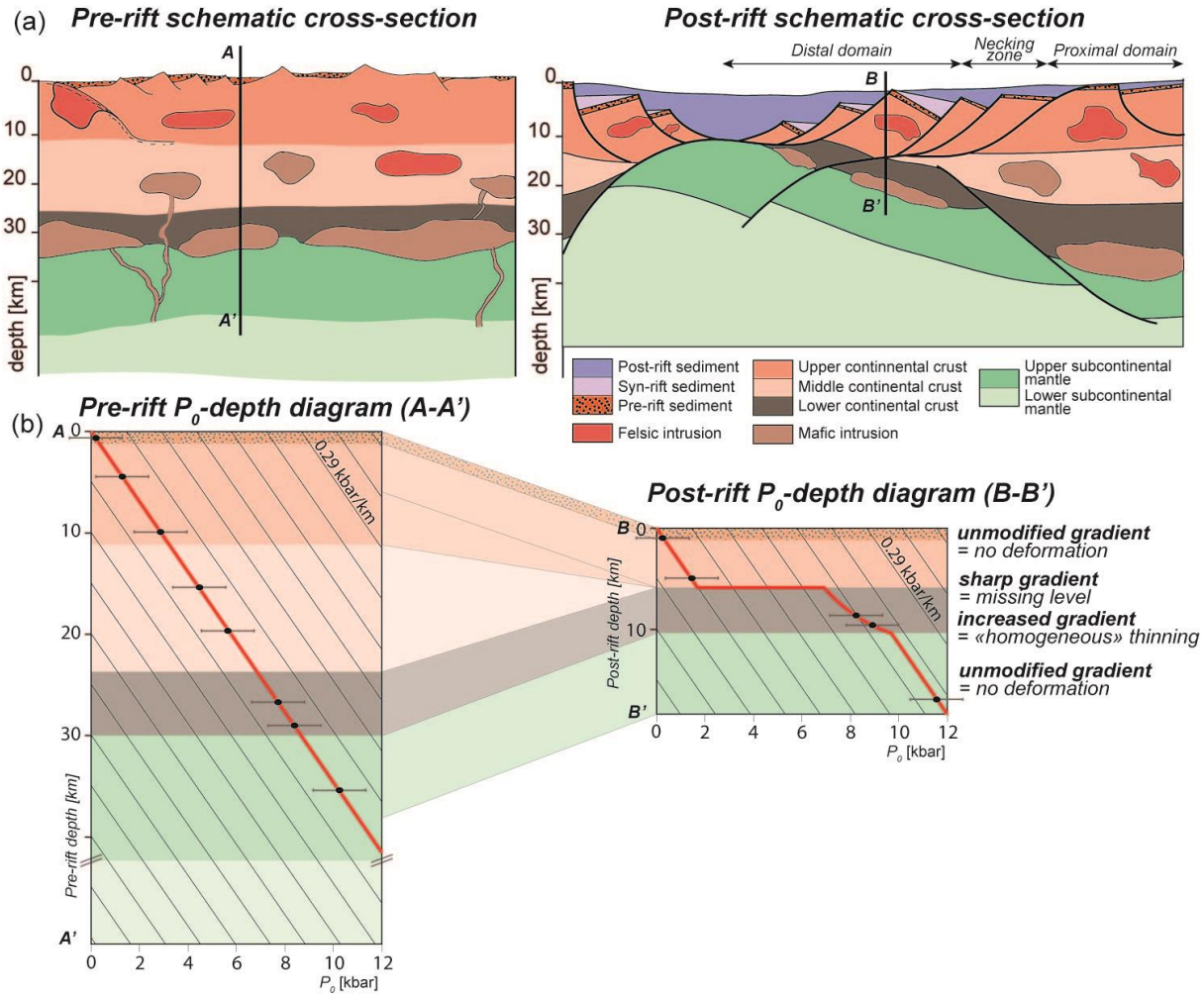

Fig. 1: (a) Pre-rift and post-rift schematic sections. Pre-rift section (modified from Mohn et al., 2010; Petri et al., 2017) illustrates the architecture of the pre-rift continental lithosphere with mafic plutons in the lower crust, mafic and felsic plutons in the middle crust and felsic plutons in the upper crust. Post-rift section (modified from Mohn et al., 2012) illustrates the general lithospheric architecture of hyper-extended rift basin. (b) Synthetic P_0-depth diagrams elaborated along a pre-rift section (A-A') and along the distal domain of a post-rift section (B-B'). The gradient is linear along the pre-rift section A-A' while different patterns are seen in post-rift section B-B': (1) unmodified gradient compared to pre-rift section in portions that escaped rift-related deformation, (2) sharp gradient in places where pre-rift crustal or lithospheric levels are missing, and (3) increased gradients when rift-related

deformation is "homogeneously" distributed across a unit. 0.29 kbar.km^{-1} is chosen as a reasonable maximum lithostatic pressure gradient (see text).

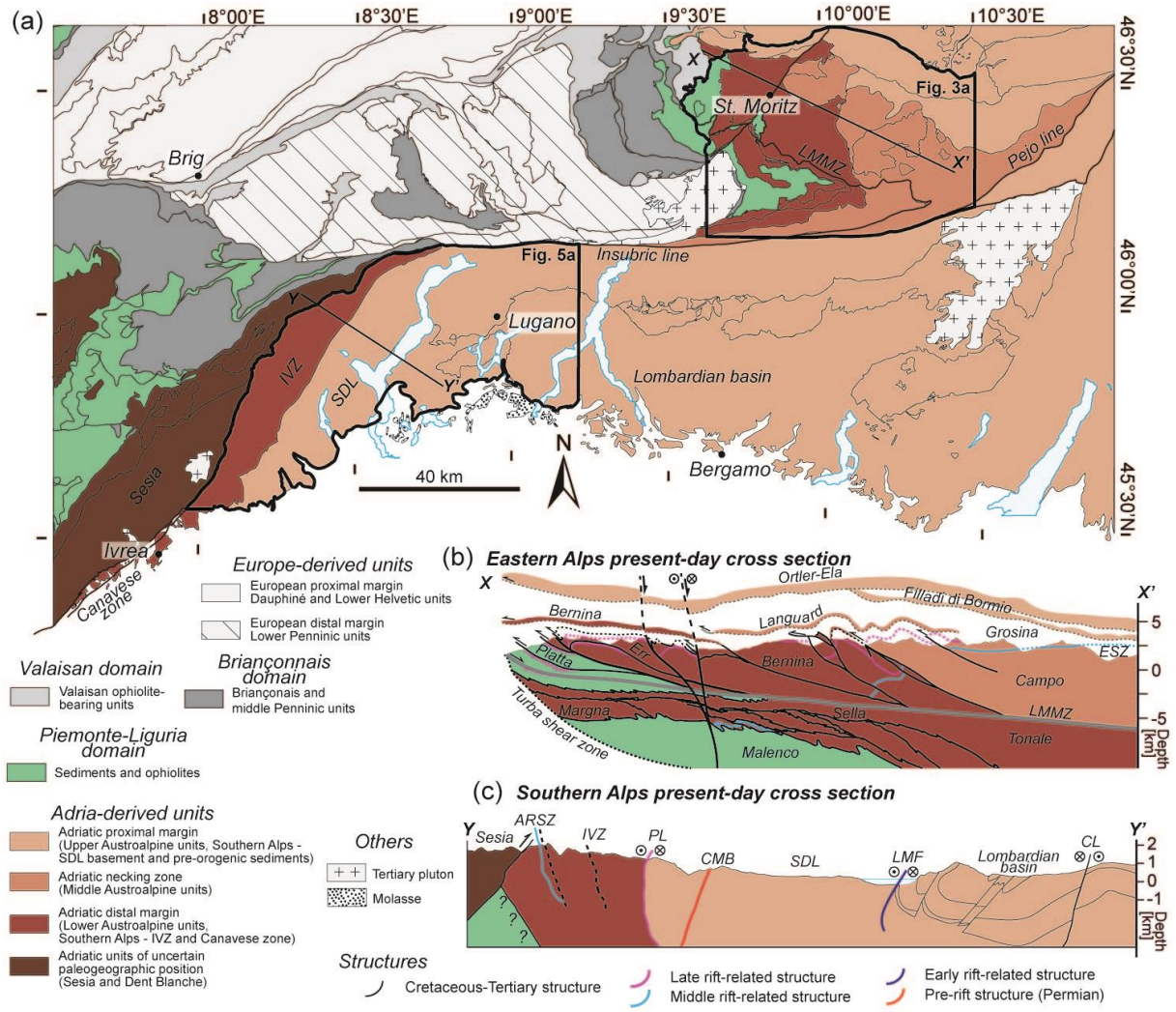

Fig. 2: (a) Tectonic map of the Southern and Central Alps compiled from the Swiss and Italian geological maps and from Müntener and Hermann (2001). (b,c) Present-day schematic cross sections across (b) the Eastern Alps (location also on Fig. 3; modified from Mohn et al., 2011) and (c) the Southern Alps (location also on Fig. 5; modified from Zingg et al., 1990). ARSZ: Anzola-Rosarolo Shear Zone; CL: Cremossina line; CMB: Cossato-Mergozo-Brissago Line; FSZ: Finero Shear Zones; IVZ; Ivrea-Verbano Zone; LMF: Lago Maggiore Fault; LVG: Lugano Val Grande Fault; LMMZ: Lunghin-Mortirolo Movement Zone; PL: Pogallo Line; SDL: Serie Dei Laghi.

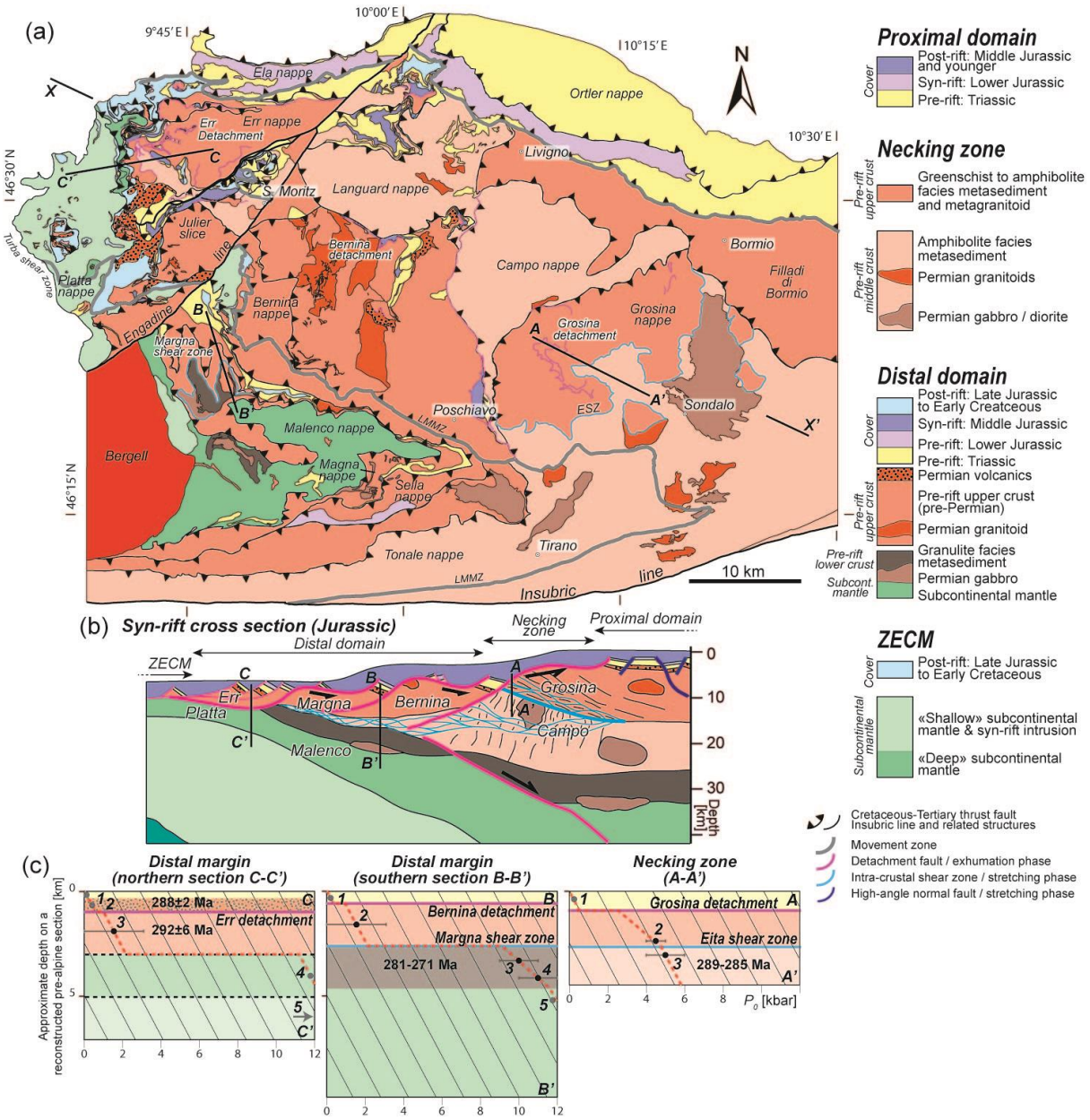

Fig. 3: Lithotectonic map of Austroalpine and Upper Penninic units in SE Switzerland and N Italy. (b) Reconstructed post-rift section modified from Mohn et al. (2012). (c) Schematic P_0-depth diagrams built using field observations, and *P-T* estimates (see text and Table S1 for references). Schematic P_0-depth diagrams are shown for the necking zone (A-A'), the southern distal section (B-B'), for the northern distal section (C-C'). Due to Alpine deformation, unit thickness is only estimated. ESZ: Eita Shear Zone; LMMZ: Lunghin-Mortirolo Movement Zone. Location of X-X' section on Fig. 2.

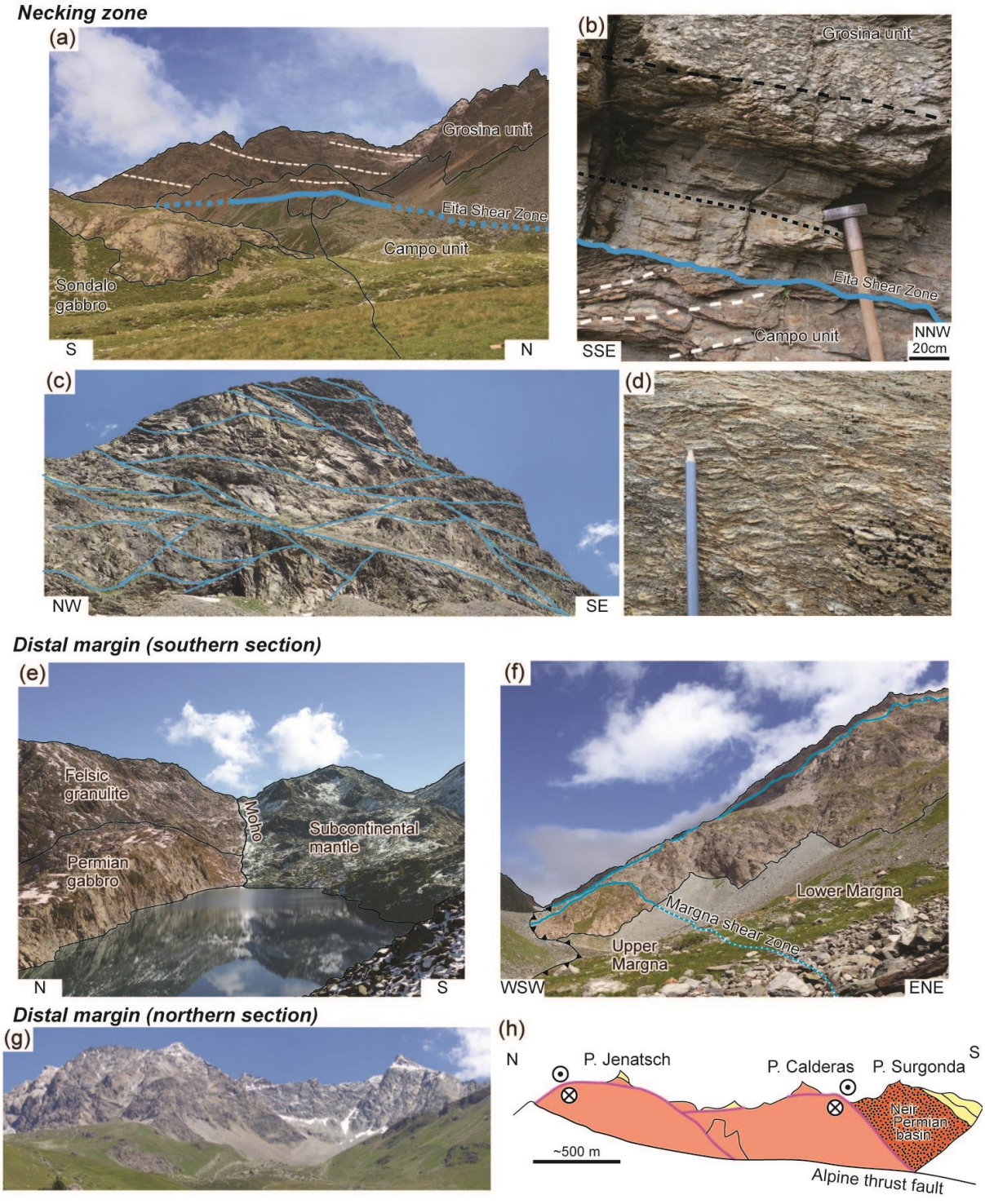

907

908 Fig. 4: Field photographs from the Eastern Alps. Necking zone: (a) panoramic view on
909 the Jurassic Eita Shear Zone (ESZ) marking the contact between the Grosina unit and the
910 Campo unit intruded by the Permian Sondalo gabbro. (b) Contact between the Campo and
911 Grosina units delimited by the Eita shear zone. (c) Anastomosing extensional shear zones
912 distributed across the entire Grosina unit. In contrast, the Campo unit is devoid of such

extensional structures. (d) Zoom of S-C structures in one of the anastomosing shear zones from the Grosina unit. Southern distal margin: (e) lower crust / upper mantle contact preserved in the Malenco unit. The pre-rift lower crust is characterized by the emplacement of the Permian Braccia gabbro; (f) the Margna shear zone in the hinge of an Alpine recumbent fold. This structure delimits the pre-rift upper crust (Upper Margna - Fora gneiss) from the pre-rift lower crust (Lower Margna - Feddoz gabbro). Northern distal margin: (g-h) panoramic view and interpreted N-S section on the Err unit and the Neir Permian basin. The geometry and localization of the Jurassic Err and Jenatsch detachment faults are at least partly controlled by the pre-rift Neir Permian basin (modified from Manatschal et al., 2015).

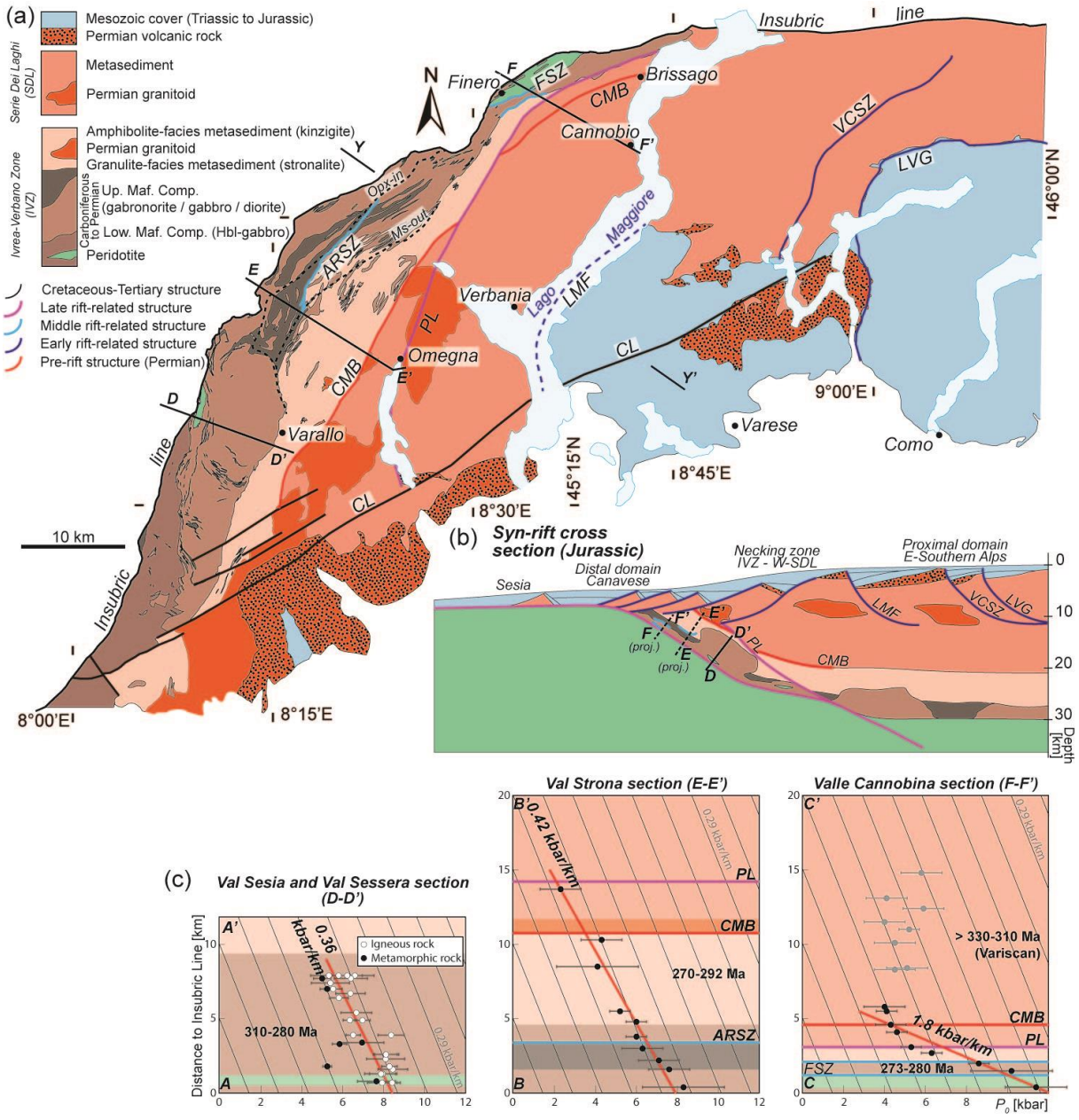

Fig. 5: (a) Lithotectonic map of the Southern Alps modified from Handy *et al.* (1999), Quick *et al.* (2003), Beltrando *et al.* (2015b) and the 1:200,000 geological maps from Italy and Switzerland. (b) Reconstructed post-rift cross-section modified from Beltrando *et al.* (2015b). (c) P_0-depth diagrams for the Val Sessera – Val Sesia section (D-D'), the Val Strona section (E-E') and the Valle Cannobina section (F-F'). The diagrams are here plotted as P_0 - distance to the Insubric line as the pre-rift IVZ is tilted to 90°, with almost no Alpine deformation. See text and Table S2 for references. ARSZ: Anzola-Rosarolo Shear Zone; CL: Cremossina Line; CMB: Cossato-Mergozo-Brissago Line; FSZ: Finero Shear Zones; LMF:

Lago Maggiore Fault; LVG: Lugano Val Grande Fault; PL: Pogallo Line; VCSZ: Val Cola Shear Zone. Location of Y-Y' section on Fig. 2.

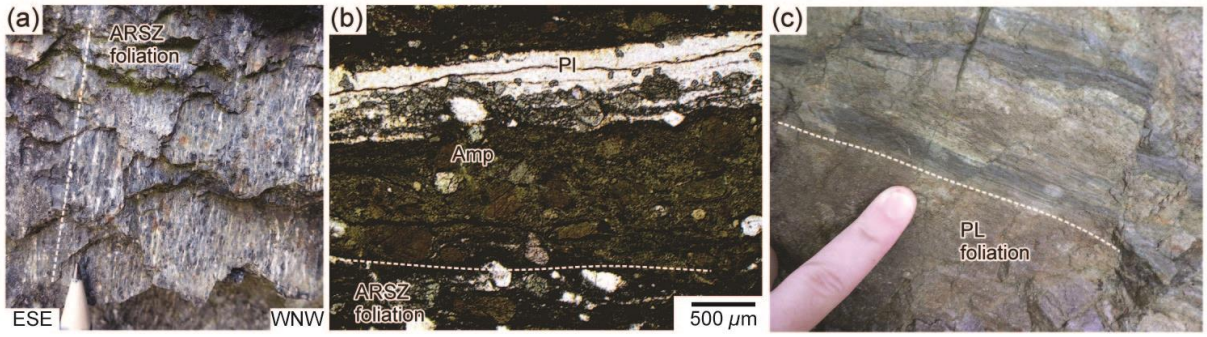

Fig. 6: Field photographs and microphotograph from the Southern Alps. (a,b) the Anzola-Rosarolo Shear Zone (ARSZ) showing dynamic recrystallization of plagioclase, amphibole and pyroxene. (c) The Pogallo line showing greenschist facies deformation.

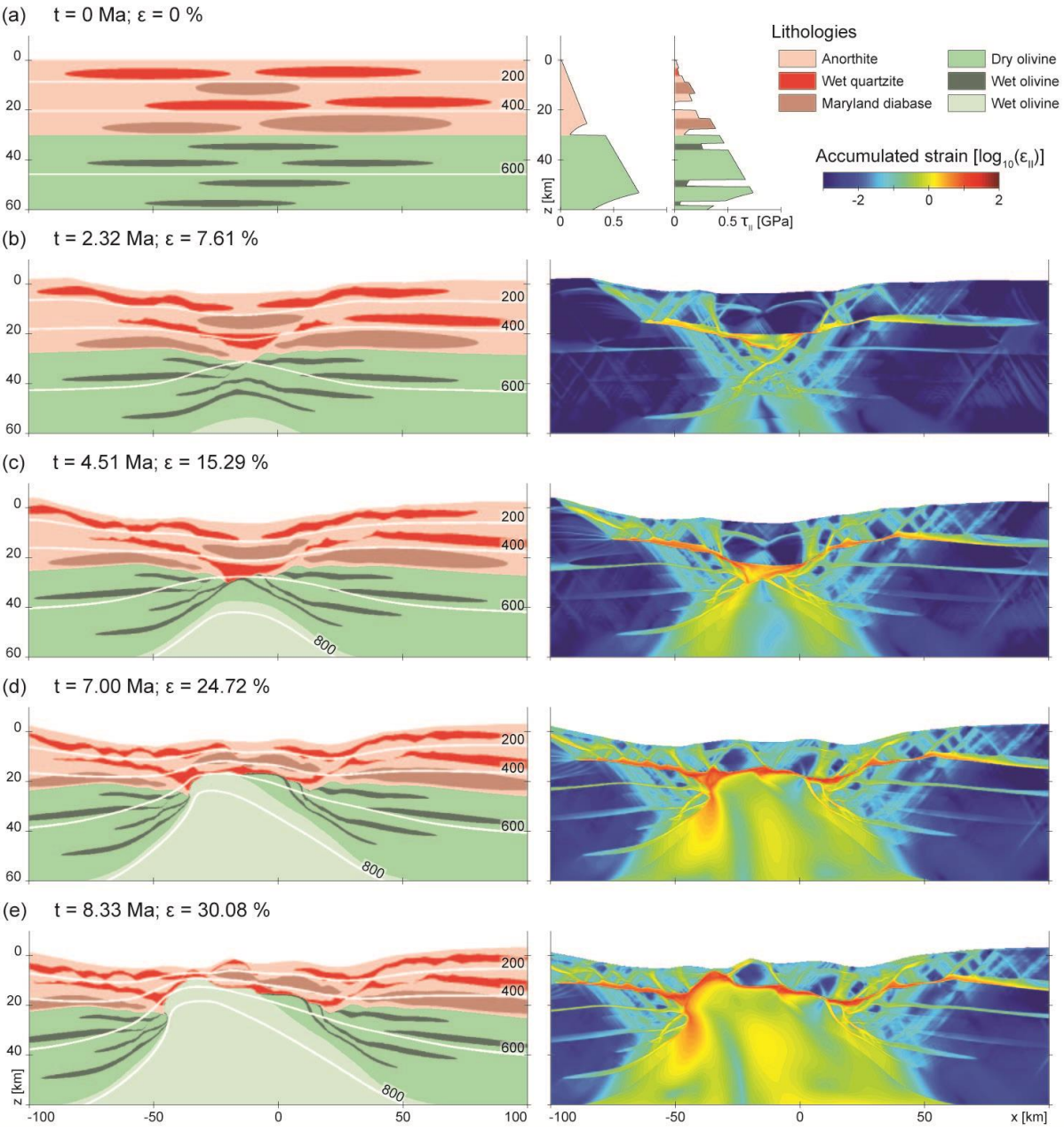

Fig. 7: Initial configuration and evolution of the reference numerical model. (a) Initial distribution of the compositional field (enlargement, left column) and initial strength profiles (right column) corresponding to a homogeneous strength profile of the lithosphere (i.e. crossing no initial heterogeneities, leftmost) and heterogeneous strength profile (x = 0 km) of the lithosphere (i.e. crossing initial heterogeneities, rightmost). Panels (b) to (e) depict the evolution of the reference model both in terms of compositional, thermal fields (left column) and accumulated strain (right column). White lines denote isotherms with 200 °C spacing. The accumulated strain was reported for the corresponding amounts of extension.

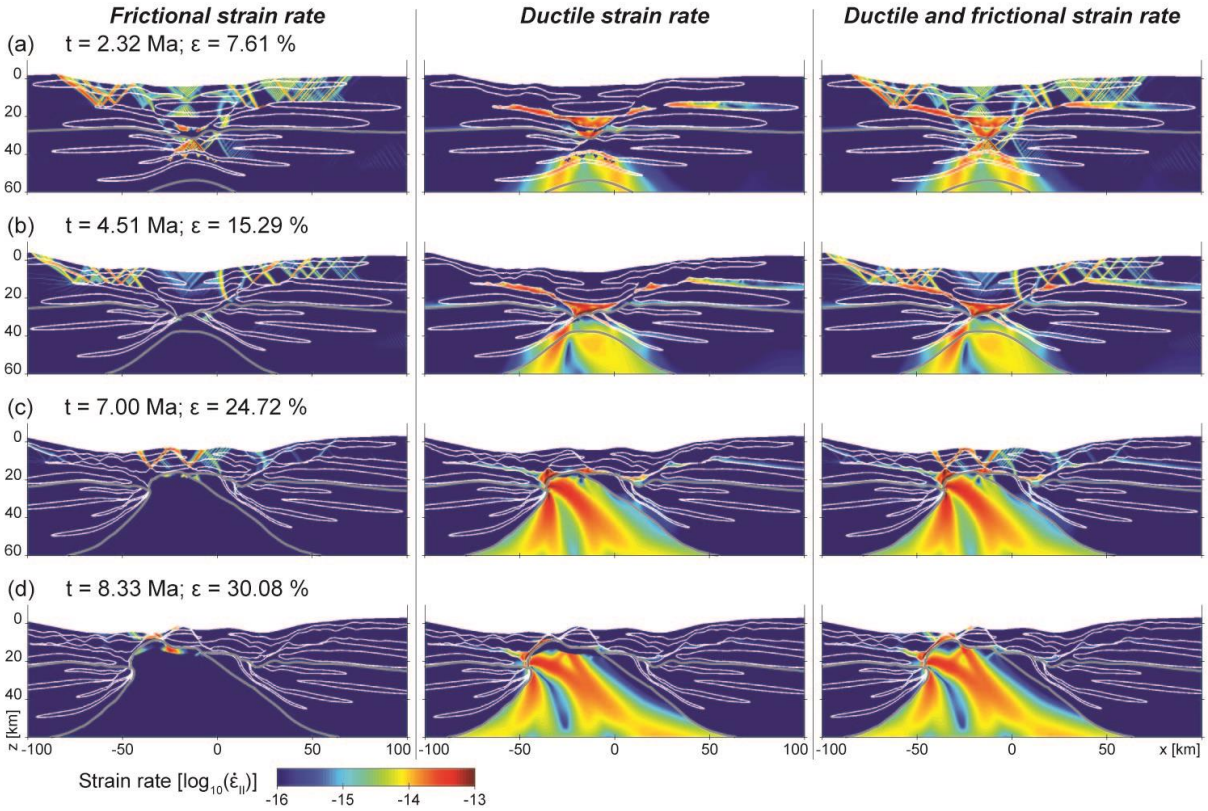

946

947 Fig. 8: Partitioning of the strain rate between the frictional (Drucker-Prager rheology)
948 and ductile rheology (viscous creep). Panels (a) to (d) correspond to a progressive time
949 evolution. The white lines correspond to the contours of heterogeneities and the grey lines
950 correspond to the Moho and the base of upper subcontinental mantle highlighting the evolving
951 morphology of the main contacts and heterogeneities.

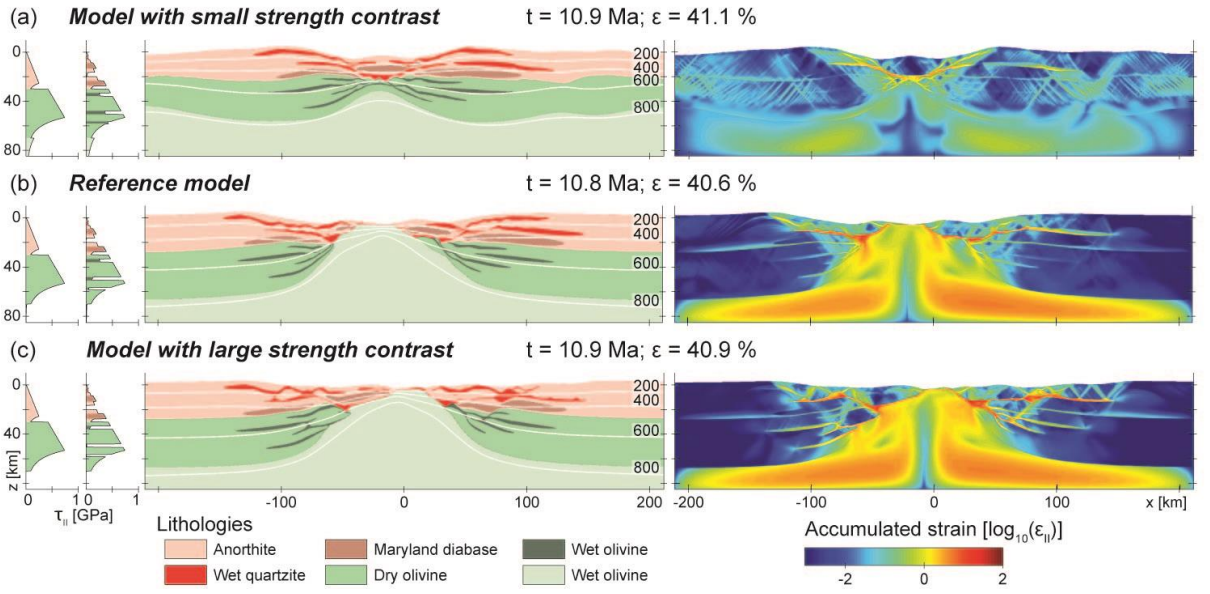

952

Fig. 9: Influence of the rheological contrasts on the style of lithospheric extension. Panel (a) corresponds to a model with reduced strength contrast compared to the reference model (see text). Panel (b) depicts the reference model. Panel (c) corresponds to a model with enlarged strength contrasts compared to the reference model. For each panel, we report initial strength profiles corresponding to lithosphere portions including heterogeneities or not (left), compositional and thermal field (isotherms depicted for each 200 °C), and the accumulated strain pattern.

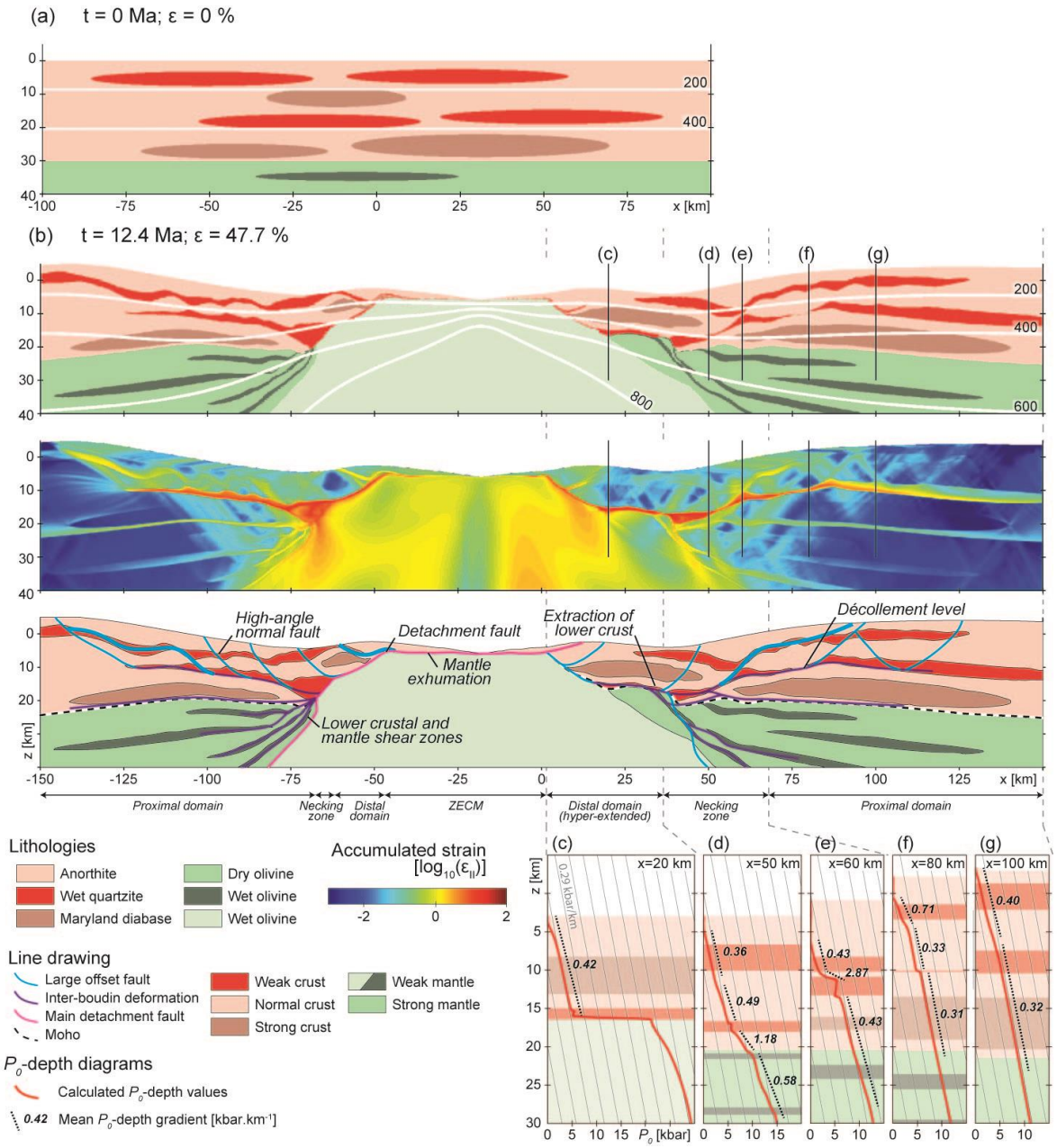

Fig. 10: (a) Pre-rift architecture of the continental lithosphere with the localization of the heterogeneities. (b) Post-rift margin architecture showing from the top to bottom: compositional and thermal fields (200 °C spacing), accumulated strain and line drawing highlighting the different recognized structures. Modeled P_0-depth diagrams and calculated gradients across (c) the distal domain, (d,e) the necking zone and (f,g) the proximal domain. ZECM: Zone of Exhumed Continental Mantle.